JOURNAL OF PROPULSION AND POWER
Vol. 21, No. 3, May–June 2005

Thrust Chamber Dynamics and Propulsive Performance of Single-Tube Pulse Detonation Engines

Fuhua Ma,* Jeong-Yeol Choi,† and Vigor Yang‡
Pennsylvania State University, University Park, Pennsylvania 16802

The modeling and simulation of the thrust chamber dynamics in an airbreathing pulse detonation engine (PDE) are conducted. The system under consideration includes a supersonic inlet, an air manifold, a valve, a single-tube combustor, and a convergent–divergent nozzle. The analysis accommodates the full conservation equations in two-dimensional coordinates and employs a chemical reaction scheme with a single-progress variable calibrated for a stoichiometric hydrogen/air mixture. The combustion and flow dynamics involved in typical PDE operations are carefully examined. In addition, a flowpath-based performance prediction model is established to estimate the theoretical limit of the engine propulsive performance. Various performance loss mechanisms, including the refilling process, nozzle flow expansion and divergence, and internal flow process are identified and quantified. The internal flow loss, which mainly arises from the shock waves within the chamber, was found to play a dominant role in degrading the PDE performance. The effects of engine operating parameters and nozzle configurations on the system dynamics are also studied in depth. Results indicate the existence of an optimum operating frequency for maximizing the performance margin. For a given cycle period and purge time, the performance increases with decreasing valve-closed time in most cases. On the other hand, a larger purge time decreases the specific thrust but increases the specific impulse for a given cycle period and valve-closed time. The nozzle throat area affects both the flow expansion process and chamber dynamics, thereby exerting a much more significant influence than the other nozzle geometrical parameters.

Nomenclature

A_e	=	area of engine exit plane
c	=	speed of sound
c_p	=	constant-pressure specific heat
E_a	=	activation energy per unit mass of reactants
e_t	=	specific total energy
F	=	axial thrust
$\boldsymbol{F}$	=	thrust vector
F_{sp}	=	specific thrust (air based)
f	=	fuel-to-air mass ratio of reactants
$\bar{f}$	=	fuel-to-air mass ratio of the mixture of reactants and purge air
g	=	gravitational acceleration
I_{sp}	=	specific impulse (fuel based)
$\boldsymbol{i}$	=	unit vector in axial direction
K	=	preexponential factor
L	=	length of detonation tube
L_{driv}	=	length of driver gas in detonation tube
M	=	Mach number
$\dot{m}_a$	=	mass flowrate of air delivered to engine
$\dot{m}_f$	=	mass flowrate of fuel delivered to combustor
$\boldsymbol{n}$	=	unit vector normal to surface
p	=	pressure
p_e	=	area-averaged pressure at engine exit plane
p_{t1}	=	total pressure at combustor entrance
q	=	heat release per unit mass of reactants
$\bar{q}$	=	heat release per unit mass of mixture of reactants and purge air
R	=	gas constant
s	=	specific entropy
T	=	temperature
T_{driv}	=	temperature of driver gas
T_{t1}	=	total temperature at combustor entrance
t	=	time
u	=	axial velocity
$\boldsymbol{u}$	=	velocity vector
u_e	=	mass-averaged axial velocity at engine exit plane
$\boldsymbol{u}_e$	=	mass-averaged velocity vector at engine exit plane
v	=	vertical velocity
x	=	axial coordinate
y	=	vertical coordinate
Z	=	mass fraction of reactants
β	=	purge-to-open time ratio, $\tau_{\text{purge}}/\tau_{\text{open}}$
γ	=	specific heat ratio
ρ	=	density
τ	=	time period
ϕ	=	equivalence ratio
$\dot{\omega}$	=	mass production rate of reactants

Subscripts

close	=	period during which valve is closed
cycle	=	pulse detonation engine operation cycle
D	=	detonation wave
driv	=	driver gas
e	=	engine exit plane
open	=	period during which valve is open
purge	=	purging stage
refill	=	refilling stage
1	=	fresh reactants upstream of detonation wave front
2	=	Chapman–Jouguet state
3	=	uniform region between chamber head end and Taylor wave
∞	=	freestream

Received 2 January 2004; revision received 19 October 2004; accepted for publication 20 October 2004.

*Postdoctoral Research Associate, Department of Mechanical Engineering; mafuhua@psu.edu.

†Visiting Assistant Professor, Department of Mechanical Engineering; juc16@psu.edu.

‡Distinguished Professor, Department of Mechanical Engineering; vigor@psu.edu. Fellow AIAA.

I. Introduction

PULSE detonation engines (PDEs) are unsteady propulsion devices that produce periodic impulse by utilizing repetitive detonations. They differ from conventional systems in two major ways:

unsteady operation and detonative combustion. A typical cycle operation of a PDE includes four basic processes: initiation of detonation wave, propagation of detonation wave, exhausting of combustion products, and refilling of reactants. Recently, PDEs have attracted considerable attention because of their potential advantages in thermodynamic cycle efficiency, hardware simplicity, operation stability, and reliability.[1,2]

Studies of PDEs have been conducted for several decades. The first reported work on intermittent detonation is attributed to Hoffman[3] in 1940. Both acetylene and benzene fuels were employed with oxygen. The work was terminated during World War II. Nicholls et al.[4] and Dunlap et al.[5] reinitiated the effort in the 1950s. They performed a series of single- and multiple-cycle detonation experiments with hydrogen/oxygen, hydrogen/air, acetylene/oxygen, and acetylene/oxygen mixtures in a 6-ft (182.9-cm) tube. In a similar setup, Krzycki[6] performed an experimental investigation using propane/air mixtures and concluded that the intermittent detonation device was not promising for propulsion applications. There is, however, doubt whether full detonation waves were realized in these devices, given the very low power output of the spark plug. Possibly due to Krzycki's conclusion, most experimental work related to PDEs was suspended in the late 1960s. Helman et al.[7] reexamined the PDE concept in the late 1980s and conducted experiments using ethylene/oxygen and ethylene/air mixtures. They employed a predetonator to initiate detonation in the main chamber and reported self-aspirating operations. Since then, there has been a growing interest in PDEs as a propulsion technology for both airbreathing and rocket systems. Several reviews are available in the literature. Eidelman et al.[8] reviewed the progress made up to the 1980s. Kailasanath conducted a series of reviews,[1,9] addressing the propulsion applications of detonation waves and several fundamental issues underlying the development of PDEs. Wu et al.[2] summarized the experimental work through 2002. More recently, a comprehensive literature survey was conducted by Ma.[10]

Serious attempts have been made to investigate the propulsive performance and flow dynamics of PDEs numerically. Most of these studies, however, were limited to either one-dimensional simulations or single-pulse operations. A major deficiency of one-dimensional analyses is that the boundary condition at the detonation tube exit, especially during the first cycle,[1] cannot be correctly specified because it depends on the local flow evolution downstream of the engine. Multidimensional analyses with computational domains including both detonation tubes and external regions are required to describe the system dynamics faithfully, especially in the near field of the tube exit where the flow is intrinsically multidimensional.[2] Multicycle operation is another important issue because of the inherently cyclic nature of PDE operation. In general, there are significant differences between single-pulse and multicycle operations; conclusions drawn from single-pulse studies may not be directly applicable to real situations with multicycle operations.[2] To date, only a limited number of multidimensional analyses of multicycle PDE operations have been reported. Kawai and Fujiwara[11] carried out two-dimensional simulations for the first two cycles of a straight tube PDE containing an argon-diluted stoichiometric hydrogen/oxygen mixture, with special attention paid to the injection behavior during the second cycle. Yungster and Perkins[12] conducted multicycle simulations of several PDE–ejector configurations with hydrogen/oxygen mixtures. Temporal variations of the thrust, impulse, and mass flow rate over five cycles were presented; however, more extended calculations may be required to reach steady periodic operation.

In view of the limitations of existing studies, a two-dimensional analysis is developed in the present paper to investigate the thrust chamber dynamics and propulsive performance of single-tube airbreathing PDEs with repetitive operation. The situation with multitube PDEs will be treated in a subsequent work.[13] In the following sections, the PDE system of concern is first described. The theoretical formulation and numerical approach are then outlined. Finally, results are presented, including the flow evolution, propulsive performance, loss mechanisms, and effects of valve timing and nozzle configuration on engine dynamics. The main objectives of this research are 1) to understand the thrust chamber dynamics in an airbreathing PDE, 2) to establish a global analysis for determining the overall propulsive performance, 3) to identify the various performance loss mechanisms, and 4) to investigate the effects of several design attributes and operating parameters on engine performance. This paper also serves as a basis for a subsequent study of the dynamics and performance of multitube PDEs.[13]

II. System Configuration and Operation

The system under consideration is shown schematically in Fig. 1. It includes a coaxial supersonic inlet with mixed compression, an air manifold, a valve, a combustion chamber consisting of single or multiple detonation tubes, and a common convergent–divergent nozzle.[2] The baseline flight condition involves an altitude of 9.3 km and a Mach number of 2.1. The freestream static pressure and temperature are 0.29 atm and 228 K, respectively, and the corresponding total pressure and temperature are 2.65 atm and 428 K.

The inlet is designed to capture and supply stable airflow at a rate demanded by the combustor and to maintain a high-pressure recovery and stability margin at various engine operating conditions. A mixed-compression inlet operating at a supercritical condition is employed in the present study.[2,14] The total pressure recovery is 84%, and the Mach number immediately in front of the terminal shock is 1.42. With the assumption of an additional 5% pressure loss across the manifold, the total pressure at the entrance of the combustor becomes 2.12 atm, where the total temperature remains at 428 K.

The present study focuses on single-tube combustor configurations; multitube designs will be treated in a companion work.[13] Injection of fuel and oxidizer and the subsequent mixing represent a critical issue in the PDE design. A correct assessment of its influence on engine dynamics and propulsive performance depends strongly on the injection strategy and local flow environment. The problem can be greatly simplified, however, without losing the major features of the cyclic operation of the PDE, by injecting premixed combustible mixture into the combustor.

Operation of the PDE is controlled by a valve located at the entrance of the combustor. Generally, there are two different modes of valve operation. One is external mode, in which the timing of the valve operation is specified externally.[2] The other is internal mode, in which the valve operation is controlled by the flow conditions inside the detonation tube, using a pre-specified threshold pressure for valve opening and a chemical sensor for valve closing.[15] In the present study, the first mode is chosen, and the valve response time is neglected for simplicity, that is, the valve is either fully closed or fully open. Furthermore, the valve open area is identical to the cross-sectional area of the detonation tube. The engine operation sequence is, thus, controlled by three time periods: the valve-closed period (τ_{close}), during which the valve is closed and the tube undergoes detonation initiation and propagation, as well as blowdown of combustion products, the purging period (τ_{purge}), during which a small amount of cold air is injected into the tube to prevent preignition of fresh reactants, and the refilling period (τ_{refill}) during which the combustible mixture is delivered to the tube. The sum of these three periods constitutes the operation cycle time: $\tau_{\text{cycle}} = \tau_{\text{close}} + \tau_{\text{purge}} + \tau_{\text{refill}}$.

Detonation initiation is one of the most challenging issues in PDE design. In general, direct initiation of detonation is impractical for repetitive operation due to difficulties resulting from the energy requirement and time response. Much effort has been applied to develop reliable and repeated low-energy initiation methods through either a deflagration-to-detonation transition process[16] or the use of a predetonator.[7,17] In the present analysis, detonation is directly

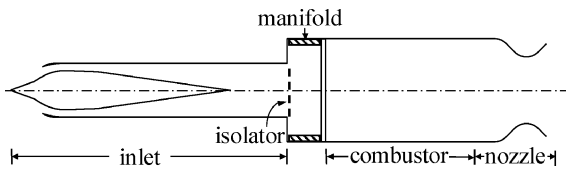

Fig. 1 Supersonic airbreathing PDE.

initiated near the head end of the chamber by a small amount driver gas to minimize the influence of detonation initiation on the assessment of engine propulsive performance.

Nozzles play a decisive role in determining the propulsive performance of a PDE. Recent studies based on numerical simulations[2,15,18] and experimental investigations[19,20] indicate that a nozzle may considerably change the thrust delivered by an engine. In addition to its influence on thrust through modification of the gas expansion process, the nozzle affects the chamber flow dynamics and, consequently, the timing of various phases of the engine operation cycle, especially for high-altitude cruise and space applications. The issue of nozzle optimization has not been resolved, due to difficulties arising from the interaction of nozzle with the other parts of the engine. Ideally, the nozzle configuration should adapt itself to the instantaneous local flow conditions. It is, however, a formidable challenge to design and fabricate such a flexible nozzle with adaptation on timescales commensurate with the PDE operation. The present work focuses on a convergent–divergent (CD) nozzle that features the following two advantages. First, the convergent section can effectively preserve the chamber pressure during the blowdown and refilling processes.[2] Second, exhaust of the high-pressure detonation products through the divergent section improves the performance due to the increase in the effective thrust wall area.

III. Theoretical Formulation

The analysis is based on the two-dimensional conservation equations of mass, momentum, and energy, and takes into account finite rate chemical kinetics. Diffusive effects are neglected because of their minor roles in determining the overall flow dynamics and propulsive performance of a PDE. If the chemical reaction rate is expressed with a single progress variable, the resultant governing equations can be written in the following vector form

$$\frac{\partial \boldsymbol{Q}}{\partial t} + \frac{\partial \boldsymbol{E}}{\partial x} + \frac{\partial \boldsymbol{F}}{\partial y} = \boldsymbol{H} \tag{1}$$

where the dependent variable vector $\boldsymbol{Q}$, convective flux vectors $\boldsymbol{E}$ and $\boldsymbol{F}$, and source vector $\boldsymbol{H}$, are defined as

$$\boldsymbol{Q} = \begin{bmatrix} \rho \\ \rho u \\ \rho v \\ \rho e_t \\ \rho Z \end{bmatrix}, \qquad \boldsymbol{E} = \begin{bmatrix} \rho u \\ \rho u^2 + p \\ \rho uv \\ u(\rho e_t + p) \\ \rho uZ \end{bmatrix}$$

$$\boldsymbol{F} = \begin{bmatrix} \rho v \\ \rho uv \\ \rho v^2 + p \\ v(\rho e_t + p) \\ \rho vZ \end{bmatrix}, \qquad \boldsymbol{H} = \begin{bmatrix} 0 \\ 0 \\ 0 \\ 0 \\ \dot{\omega} \end{bmatrix} \tag{2}$$

In the preceding equations, ρ, u, v, e_t, and Z represent the density, axial velocity, vertical velocity, specific total energy, and progress variable, that is, mass fraction of reactants, respectively. The pressure p is obtained through the equation of state,

$$p = (\gamma - 1)\rho[e_t - (u^2 + v^2)/2 - Zq] \tag{3}$$

For a one-step, irreversible reaction, the mass production rate of reactants $\dot{\omega}$ is

$$\dot{\omega} = -K\rho Z \exp(-E_a/RT) \tag{4}$$

The five parameters involved in Eqs. (3) and (4) for a stoichiometric hydrogen/air system are chosen to be $\gamma = 1.290$, $R = 368.9$ J/(kg · K), $q = 2.720 \times 10^6$ J/kg, $E_a = 4.794 \times 10^6$ J/kg, and $K = 7.5 \times 10^9$ s^{-1}. The first three thermodynamic parameters are optimized by comparing the calculated detonation wave properties with those obtained from the NASA chemical equilibrium analysis.[21] The relative errors are less than 5% in terms of the detonation velocity and the Chapman–Jouguet (CJ) pressure and temperature. The remaining two chemical kinetic parameters, E_a and K, are adopted from Ref. 22. Their primary influence appears in the internal structure of a detonation wave front, and the effect on the overall flow evolution and propulsive performance is relatively minor. The employment of single values of γ and R for the purge gas, reactants, and products inevitably introduces certain errors. The performance trends and resultant conclusions, however, are not affected in terms of the effects of operation timing and nozzle configuration.

IV. Numerical Approach

The governing equations outlined in the preceding section are solved numerically using a recently developed space–time conservation-element/solution-element method.[23,24] The scheme offers many unique features, such as a unified treatment of space and time, introduction of solution and conservation elements to construct a simple stencil, treatment of dependent variables and their derivatives as independent variables to be solved simultaneously, and no interpolation or extrapolation required to evaluate fluxes at cell interfaces. Furthermore, it has extremely low numerical dissipation and dispersion errors and, thus, circumvents the deficiencies of existing numerical methods for treating detonation waves and shock discontinuities.

In a chemically reacting flow, the timescales associated with chemical reactions are much smaller than those of flow evolution. This produces the well-known stiffness problem. The ensuing numerical difficulty can be treated using a sub-time step technique, as detailed in Ref. 24. The computer code is equipped with a two-dimensional unstructured triangular mesh solver to facilitate calculations with complex geometries. Further efficiency is achieved by parallelizing the code based on the message-passing-interface library and a domain-decomposition technique.[25] The entire analysis has been validated against a series of detonation problems for which either analytical solutions or experimental data are available.[2,24]

V. Results and Discussions

Calculations were first conducted for the baseline configuration, as shown schematically in Fig. 2. The detonation tube measures 60 cm in length and 16 cm in height. The nozzle has a length of 20 cm and a throat height of 12 cm, along with a convergent half-angle of 45 deg and a divergent half-angle of 15 deg. An external region is included in the computation to circumvent the difficulty of specifying boundary conditions at the nozzle exit. The entire domain is discretized into 554,228 unstructured triangular grid cells, of which 320,000 are located in the detonation tube; 88,080 are in the nozzle; and 146,168 are in the external region. This dense grid permits accurate resolution of detonation propagation in the axial direction, according to a grid independence analysis for the flow evolution in the chamber.[10] The cell size near the head end is about 0.2 mm in the axial direction and 2 mm in the vertical direction. It increases to about 5 mm in both directions at the external boundary. The computational domain is decomposed into 64 subdomains using the METIS software[25] for parallel computing. The Courant–Friedrichs–Lewy number used is 0.5, and the corresponding time step is about 5×10^{-5} ms.

The boundary conditions at the head end of the detonation tube are specified according to the stage in the engine operation cycle. It is modeled as a rigid wall when the valve is closed. During the

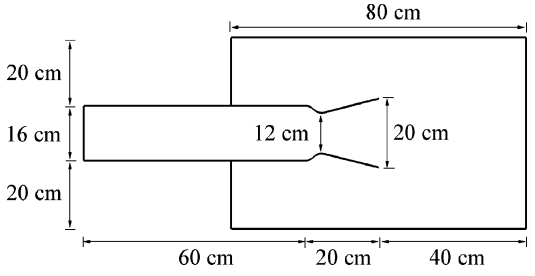

Fig. 2 Computational domain for single-tube PDE.

purging stage, the total temperature and total pressure are specified as 428 K and 2.12 atm, respectively, as mentioned in Sec. II. The axial velocity is extrapolated from the interior points, and the reactant mass fraction is set to zero. The same conditions are used during the refilling stage, except that the reactant mass fraction is set to unity. A nonreflecting boundary condition is implemented along the open boundary of the external region.[23]

The detonation tube is initially filled with a stoichiometric hydrogen/air mixture at the ambient pressure (0.29 atm) and temperature (228 K). Detonation is initiated by a small amount of driver gas at 2000 K and 30 atm near the head end. This region is set to be very short, 0.02 cm, to minimize its effect on the assessment of the engine propulsive performance. The thermal energy of the ignition source per unit cross-sectional area is approximated as

$$c_p T_{\text{driv}} \rho_{\text{driv}} L_{\text{driv}} = [\gamma/(\gamma-1)] p_{\text{driv}} L_{\text{driv}} \approx 0.27\ \text{J/cm}^2 \qquad (5)$$

This value can be compared with the thermal energy released during the detonation of the reactants within the tube,

$$\frac{c_p T_{\text{driv}} \rho_{\text{driv}} L_{\text{driv}}}{q \rho L} = \frac{[\gamma/(\gamma-1)] p_{\text{driv}} L_{\text{driv}}}{[q/(RT)] p L} \approx 0.5\% \qquad (6)$$

The net effect on the system performance appears to be limited.

A. Flow Evolution

A series of analyses was conducted over a wide range of operating parameters. The baseline case has a cycle period (τ_{cycle}) of 3 ms, a valve-closed time (τ_{close}) of 2.1 ms, and a purge time (τ_{purge}) of 0.1 ms. The ambient flow is treated as stationary. Figures 3 and 4, respectively, show the time evolution of the Mach number and density gradient fields during the first cycle of operation. The corresponding pressure and Mach number distributions along the centerline of the

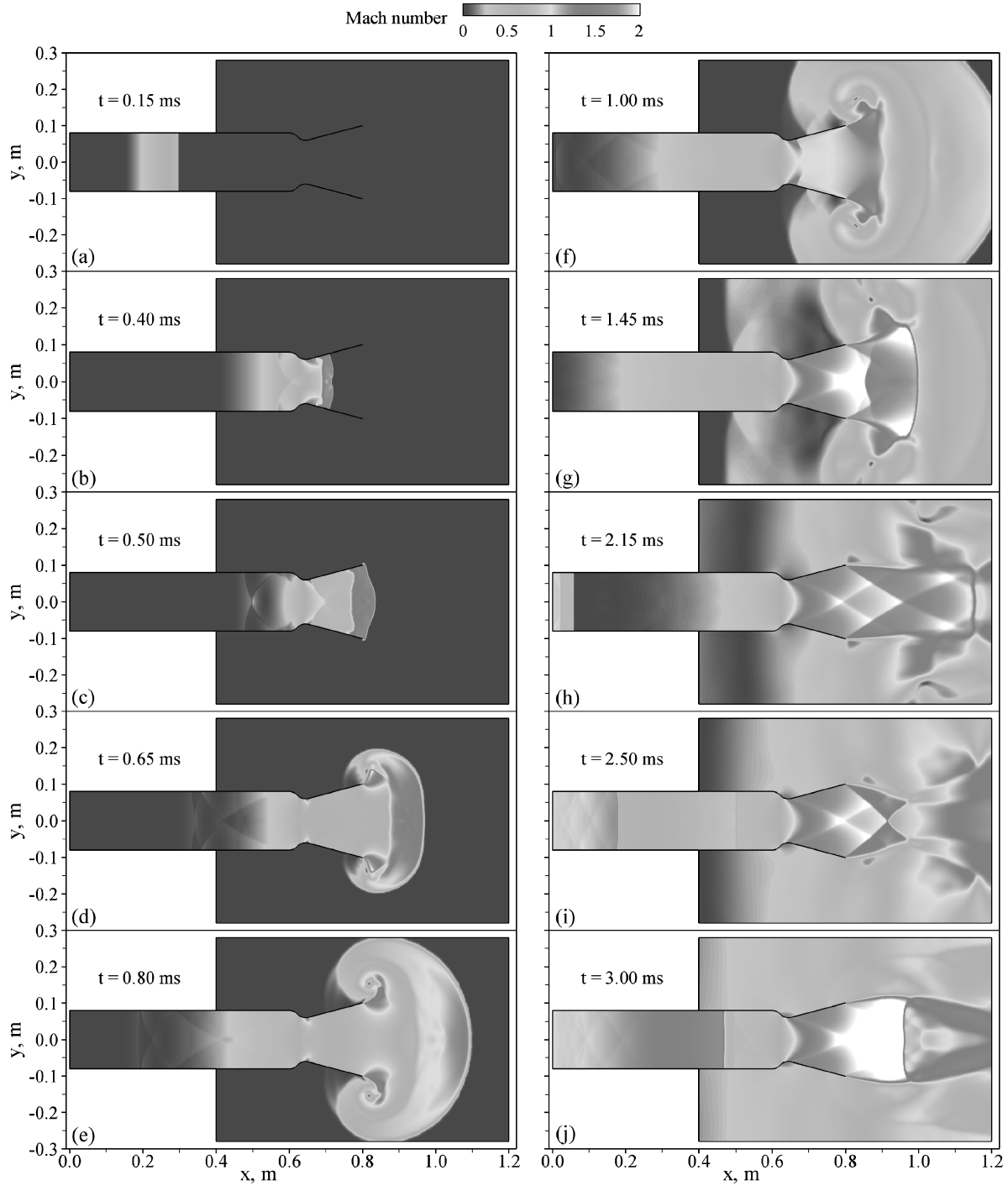

Fig. 3 Time evolution of Mach number field during first cycle of operation ($\tau_{\text{cycle}} = 3$ ms and $\tau_{\text{close}} = 2.1$ ms).

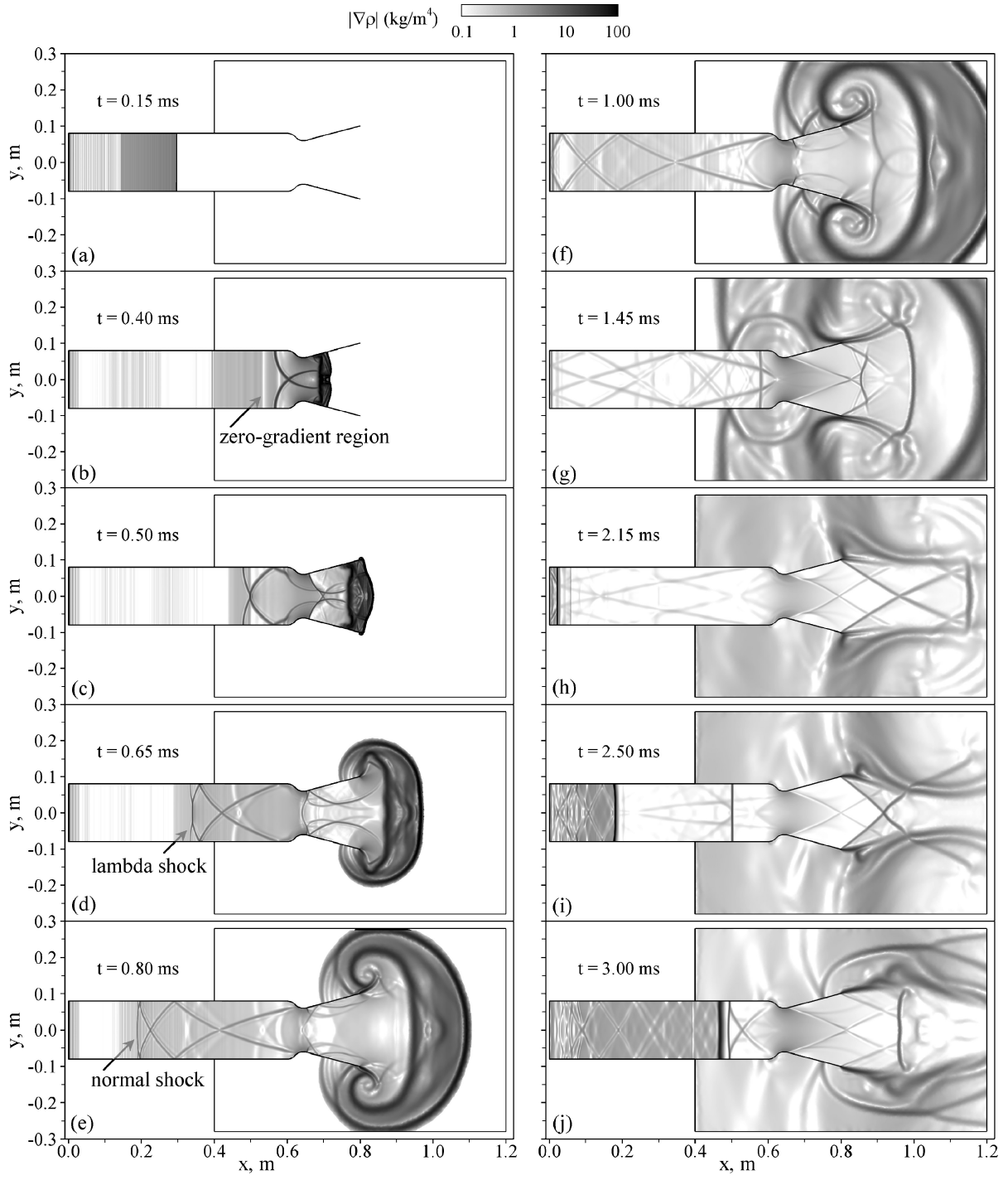

Fig. 4 Time evolution of density-gradient field during first cycle of operation ($\tau_{cycle} = 3$ ms and $\tau_{close} = 2.1$ ms).

computational domain are displayed in Fig. 5. Figure 6 shows the time histories of the pressure and Mach number at the centers of the head end, nozzle throat, and nozzle exit.

Initially, the detonation tube is filled with reactants, and the valve is closed. Detonation is then initiated by the driver gas near the head end and propagates downstream toward the unburned mixture. It is followed by a centered rarefaction wave known as the Taylor wave,[26] which decreases the pressure and brings the flow to rest to satisfy the stationary condition at the head end. A uniform region with constant flow properties exists between the chamber head end and the rear end of the Taylor wave. A detailed discussion of the wave evolution is given by Wu et al.[2] using a numerically obtained x–t diagram. The detonation wave speed u_D, Mach number M_D, and the flow properties at the CJ point can be analytically obtained according to the CJ theory. The flow properties in the uniform region can be related to the CJ properties with the Riemann invariants relation and the isentropic relation across the Taylor wave (see Refs. 27 and 28). The resultant analytical formulas are summarized as follows:

$$M_D = \sqrt{\frac{\gamma^2-1}{2\gamma}\frac{q}{RT_1}} + \sqrt{\frac{\gamma^2-1}{2\gamma}\frac{q}{RT_1}+1}$$

$$u_D = M_D\sqrt{\gamma RT_1} \tag{7}$$

$$M_2 = \frac{M_D^2-1}{\gamma M_D^2+1}, \qquad \frac{p_2}{p_1} = \frac{1+\gamma M_D^2}{1+\gamma}$$

$$\frac{T_2}{T_1} = \left(\frac{1+\gamma M_D^2}{(1+\gamma)M_D}\right)^2 \tag{8}$$

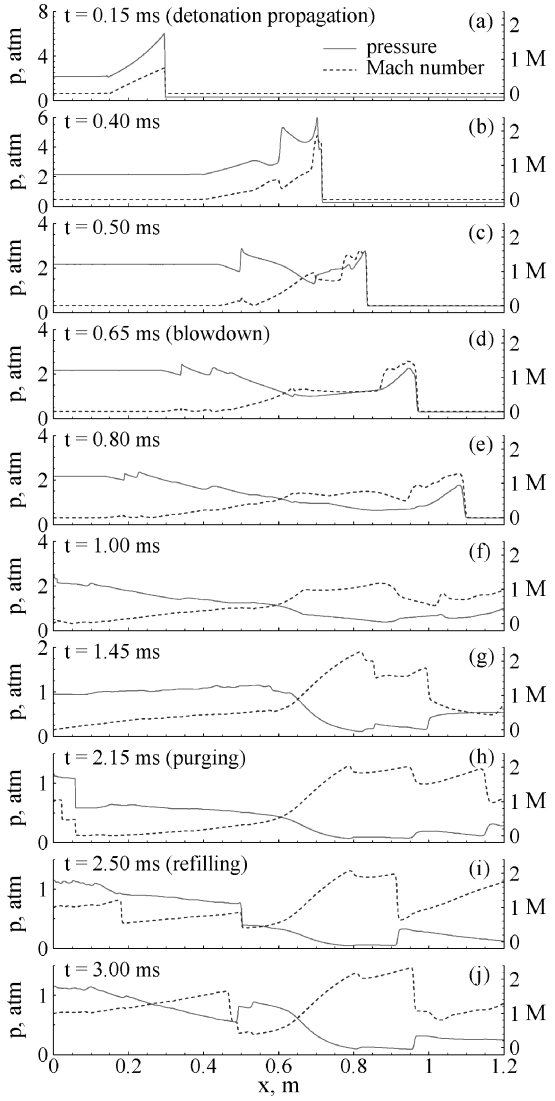

Fig. 5 Time evolution of ——, pressure and – – –, Mach number distributions along centerline during first cycle of operation ($\tau_{cycle} = 3$ ms and $\tau_{close} = 2.1$ ms).

$$\frac{p_3}{p_2} = \left(1 - \frac{\gamma - 1}{2}\frac{M_D^2 - 1}{\gamma M_D^2 + 1}\right)^{2\gamma/(\gamma-1)}$$

$$\frac{T_3}{T_2} = \left(1 - \frac{\gamma - 1}{2}\frac{M_D^2 - 1}{\gamma M_D^2 + 1}\right)^{2} \tag{9}$$

where subscripts 1, 2, and 3 represent the unburned gas, the CJ point, and the uniform region, respectively. Equation (7) yields a detonation wave Mach number of 5.94 and speed of 1956 m/s, which agrees well with the value of 1950 m/s obtained from the NASA CEA code.[21] The simulated flow properties at the CJ point and in the uniform region also closely match the analytical predictions. The deviation is less than 0.1% for the CJ properties and 0.4% for the uniform region properties, as shown in Table 1.

At $t = 0.15$ ms, the detonation wave travels to $x = 29.5$ cm and the uniform region extends to 15.0 cm. These two lengths deviate slightly (0.6%) from the following analytical predictions, due to the effect of the detonation initiation process.

$$x_D = u_D \times t = 1956 \text{ m/s} \times 0.15 \text{ ms} = 29.3 \text{ cm} \tag{10}$$

$$x_3 = c_3 \times t = 1006 \text{ m/s} \times 0.15 \text{ ms} = 15.1 \text{ cm} \tag{11}$$

where c_3 is the sound speed in the uniform region. Generally, the uniform region is about halfway between the detonation wave front

Table 1 Flow properties at CJ point and in uniform region[a]

Property	Numerical	Analytical	CEA[21]
u_D, m/s	1956	1956	1950
p_2, atm	5.855	5.888	5.798
T_2, K	2663	2665	2853
M_2	0.737	0.737	0.821
p_3, atm	2.158	2.154	——
T_3, K	2133	2126	——
c_3, m/s	1007	1006	——

[a] $T_1 = 228$ K, $p_1 = 0.29$ atm, $\gamma = 1.29$, $R = 368.9$ J/(kg · K), and $q = 2.72 \times 10^6$ J/kg.

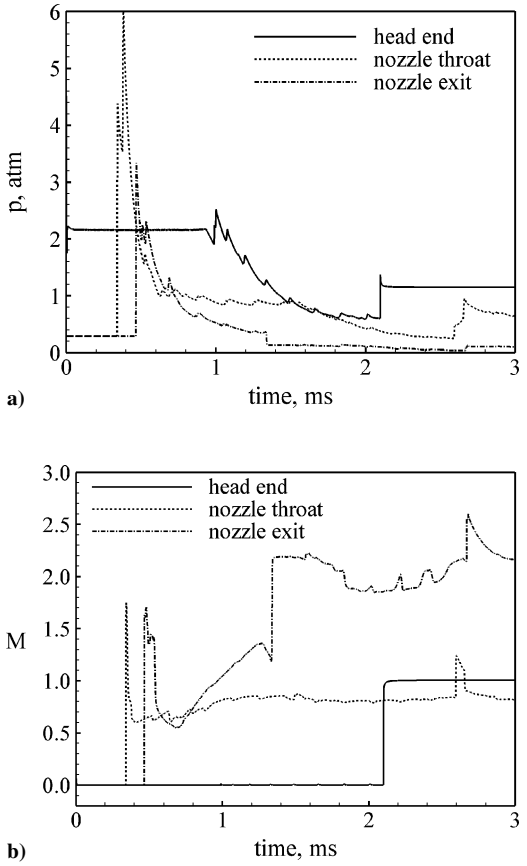

Fig. 6 Time histories of a) pressure and b) Mach number at centers of head end, nozzle throat, and nozzle exit during first cycle of operation ($\tau_{cycle} = 3$ ms and $\tau_{close} = 2.1$ ms).

and the head end,[27] as shown by the following relation:

$$\frac{c_3}{u_D} = \frac{\sqrt{\gamma R T_3}}{M_D \sqrt{\gamma R T_1}} = \frac{M_D^2 + 1}{2M_D^2} \approx \frac{1}{2} \tag{12}$$

The detonation wave travels downstream and reaches the reactant/air interface at the tube exit at $t = 0.305$ ms. It then degenerates to a nonreacting shock wave, that is, the primary shock wave, due to the lack of energy supplied from fresh reactants. Meanwhile, a series of expansion waves are generated and propagate upstream. The primary shock wave further reflects from the convergent wall. Its propagation through the nozzle throat resembles shock diffraction over a convex curved wall.[29] At $t = 0.40$ ms, the primary shock wave reaches the divergent section and is curved under the effects of the expansion waves originating from the wall, and the two reflected shock waves intersect with each other. Along the wall, the flow behind the primary shock is locally expanded to become supersonic, which leads to the formation of two shock waves stemming out from the wall, as seen clearly in the close-up view of the pressure field in Fig. 7a. On the other hand, the interaction between the upstream-traveling expansion waves and the downstream-traveling

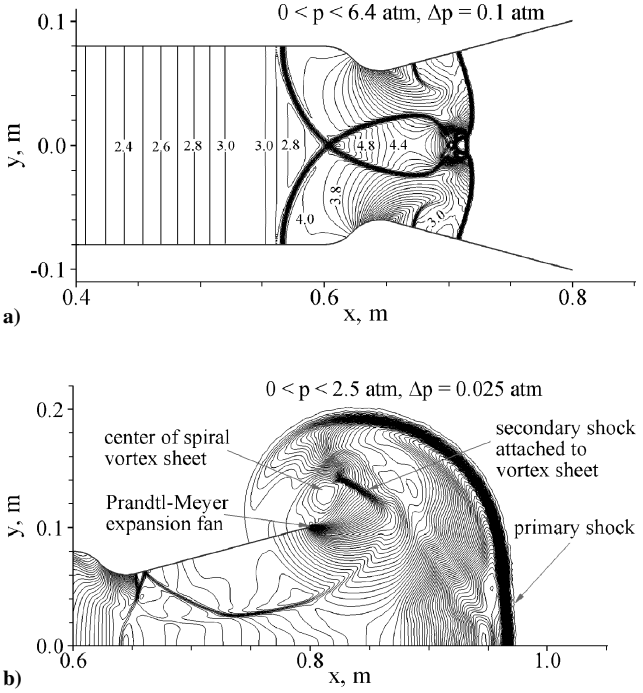

Fig. 7 Close-up views of pressure contours in nozzle at a) $t = 0.40$ and b) $t = 0.65$ ms.

Taylor wave causes a small zero-gradient region, as evidenced by the blank region located at about $x = 53$ cm in Fig. 4b and by the pressure contours in Fig. 7a.

At $t = 0.50$ ms, the primary shock wave arrives at the nozzle exit. The pressure and temperature on the centerline immediately behind the shock wave are 2.76 atm and 527 K, respectively, corresponding to a shock Mach number[30] of 2.93, which is much smaller than the original detonation Mach number of 5.94. Within the detonation tube, the upstream-traveling expansion waves pass through the downstream-traveling Taylor wave, and the uniform region begins to shrink. The two reflected shock waves intersect with each other, propagate further upstream, hit, and then reflect off of the tube walls. This leads to the formation of a more complicated shock wave structure.

At $t = 0.65$ ms, the primary shock wave has moved out of the nozzle. The shock Mach number is 2.53 at the centerline and decreases to about unity near the wall due to strong flow expansion around the edge of the nozzle exit. The phenomenon is consistent with Skews' study[31] on the shock diffraction over a sharp corner, in which the shock Mach number near the wall approaches unity for large corner angles. On the other hand, owing to the velocity difference between the exhaust and ambient flows, slip lines (or vortex sheets) form and roll up (Figs. 4e and 4f). At $t = 0.65$ ms, the center of the upper spiral vortex sheet is positioned at $x = 0.811$ m and $y = 0.136$ m, at which the flow is stationary and has a pressure as low as 0.18 atm. A quantitative analysis on vorticity production in shock diffraction was recently conducted by Sun and Takayama.[32] In the inner region near the edge of the nozzle exit, the flow accelerates from subsonic to sonic due to the expansion waves emanating from the edge, and finally a Prandtl–Meyer expansion fan is formed (Fig. 7b). The expanded supersonic flow is terminated by a downstream secondary shock attached to the vortex sheet. Although the flow structure resembles that of shock diffraction over a sharp corner,[32,33] it is complicated by the flow nonuniformity resulting from the detonation wave and contact surface. Within the detonation tube, the shock waves interact and reflect off of the tube walls, forming a lambda-shock structure (Fig. 4d) and eventually a nearly normal leading shock wave (Fig. 4e).

At $t = 1.00$ ms, part of the primary shock wave has moved out of the computational domain. The centers of the spiral vortex sheets are shifted slowly to the position of (0.829 m, ±0.175 m), whereas the pressure further decreases to 0.07 atm. The secondary shocks attached to the vortex sheets begin to interact. The Prandtl–Meyer expansion fans originating from the edges still exist, and the pressure at the nozzle exit plane is about 0.48 atm, higher than the ambient value of 0.29 atm. The nozzle flow remains underexpanded. In the vicinity of the nozzle throat, the sonic region expands from the wall to the entire throat section. The curved sonic line (Fig. 3f) starts at the wall slightly upstream of the throat and crosses the nozzle centerline downstream of the throat.[30] The Mach number at the center of the nozzle throat is less than unity (Fig. 6b). Along the centerline downstream of the sonic line, the flow remains slightly below sonic and then accelerates to become supersonic near the exit plane due to the expansion waves emanating from the edge of the nozzle exit (Fig. 5f). The Mach number at the center of the nozzle exit plane is about 1.05. Inside the detonation tube, the upstream-traveling expansion waves and leading shock wave have reached the head end and have been reflected off, terminating the head-end pressure plateau that remained until $t = 0.935$ ms. The head-end pressure then decays gradually, followed by an abrupt increase, as shown in Fig. 6a. The zigzag pressure history at the head end between 1 and 2 ms results from the reflection of the subsequent upstream-traveling expansion waves and shock waves from the head end.

As the blowdown process continues, the pressure within the tube and nozzle decays. At $t = 1.45$ ms, the nozzle flow has developed to be overexpanded, with the exit pressure decreasing to 0.13 atm at the center and 0.21 atm at the wall. Also, the Prandtl–Meyer expansion fans disappear and oblique shocks form near the edges of the nozzle exit. Within the nozzle, the flow downstream of the curved sonic line becomes supersonic, and the Mach number at the center of the nozzle exit is about 2.2.

The valve opens at $t = 2.10$ ms and the purging process begins. The head-end pressure is about 0.6 atm before the valve opening, whereas the total pressure at the combustor entrance is 2.12 atm. As a result of this large pressure difference, a right-running shock wave is established along with a contact surface between the burned and the purge gases (Figs. 3h and 4h). The temperature increases from 370 to 1916 K across the contact surface, and the Mach number decreases from 1.04 to 0.46. Another contact surface forms between the fresh reactants and the purge air when the refilling process commences 0.1 ms later. The corresponding refilling pressure and velocity are 1.16 atm and 423 m/s, respectively. At $t = 2.50$ ms, the shock wave and the two contact surfaces travel to 0.5, 0.18, and 0.13 m, respectively. The pressure at the nozzle exit decays to 0.06 atm. The external flow structure bears a close resemblance to that of an overexpanded nozzle flow at a steady-state condition.[30] The oblique shocks intersect with each other and reflect off of the slip lines (or shear layers) to generate expansion waves (Fig. 4i). A Mach intersection[30] of the two oblique shocks occurs as the intersection point moves upstream with a further decay of the nozzle exit pressure.

At the end of the first cycle ($t = 3.0$ ms), the shock wave resulting from the valve opening moves out of the nozzle and interacts with the existing waves, further complicating the external flowfield. The fresh reactants fill the tube to about two-thirds of the length. The pressure of the reactants ranges from 1.16 atm at the head end to 0.60 atm at the leading point, which is significantly higher than the ambient pressure of 0.29 atm. The velocity of the reactants varies from 430 to 600 m/s, in contrast to the initial stationary condition.

The engine rapidly reaches a steady periodic operation as the cycle repeats. Figure 8 shows the time history of the head-end pressure during the first five cycles. Significant differences between the first and later cycles are observed. The pressure plateau during the first 0.935 ms does not appear in later cycles because of the rarefaction of waves from the previous cycle. In addition, the higher pressure of the refilled reactants in later cycles leads to a higher head-end pressure immediately after detonation. Figure 9 shows the specific impulse for five cycles, along with the filling length, defined as the length at which the detonation wave catches the leading fresh reactants. The specific impulse increases rapidly due to the increasing loading

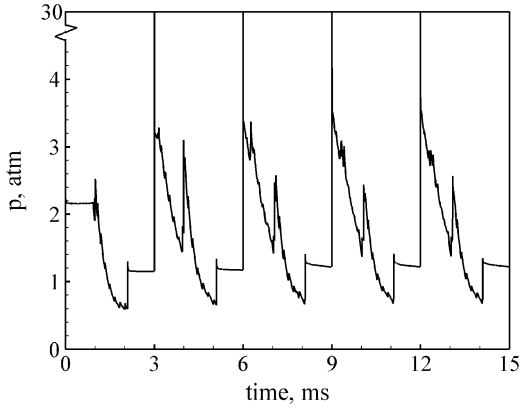

Fig. 8 Time history of head-end pressure during first five cycles ($\tau_{cycle} = 3$ ms and $\tau_{close} = 2.1$ ms).

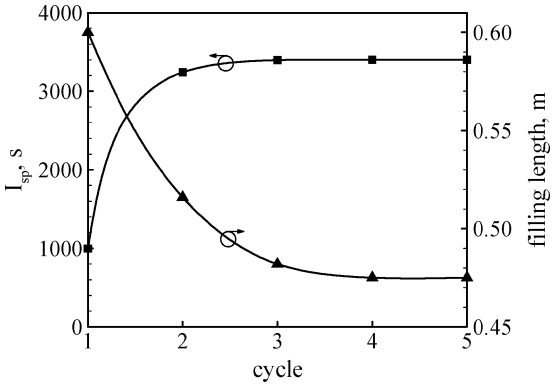

Fig. 9 Specific impulse and filling length of first five cycles ($\tau_{cycle} = 3$ ms and $\tau_{close} = 2.1$ ms).

density of the reactants and reaches 3402 s at the fifth cycle. The corresponding filling length is 47.5 cm, about 80% of the chamber length.

Figure 10 shows the time evolution of the density-gradient field during the fifth cycle, at which steady cyclic operation has been achieved. Although the valve timing is identical to that of the first cycle, the flow structure differs substantially due to the flow nonuniformity arising from the previous cycle. (See Fig. 4 for comparison.) The high reactant-flow speed (about 500 m/s) causes the detonation wave to propagate faster to the tube exit. It travels 36.8 cm within 0.15 ms from initiation (Fig. 10a), in contrast to 29.5 cm in the first cycle. Figure 11 shows the time history of the pressure at the center of the nozzle exit. The flow is overexpanded from 12.0 to 12.3 ms and from 12.9 to 15.0 ms, in contrast to about 1.6 ms of overexpansion during the first cycle. The Mach number at the center of the nozzle exit remains supersonic throughout the whole cycle. The time evolution of the Mach number field (not shown) suggests that

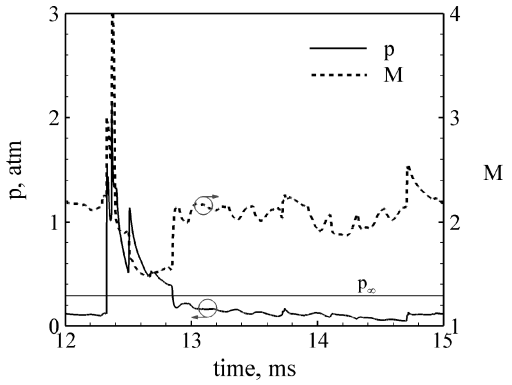

Fig. 11 Time histories of pressure and Mach number at center of nozzle exit during steady periodic operation (fifth cycle, $\tau_{cycle} = 3$ ms, and $\tau_{close} = 2.1$ ms).

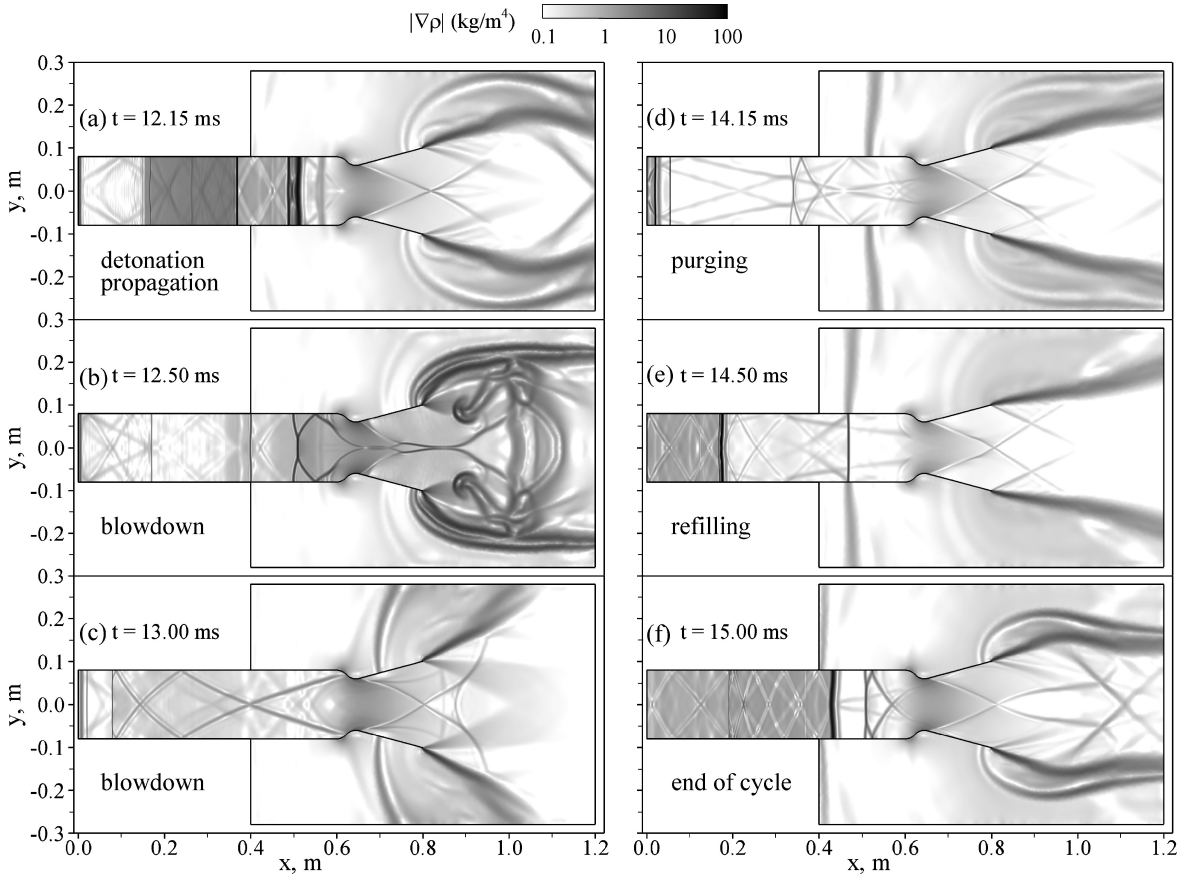

Fig. 10 Time evolution of density-gradient field during steady periodic operation (fifth cycle, $\tau_{cycle} = 3$ ms, and $\tau_{close} = 2.1$ ms).

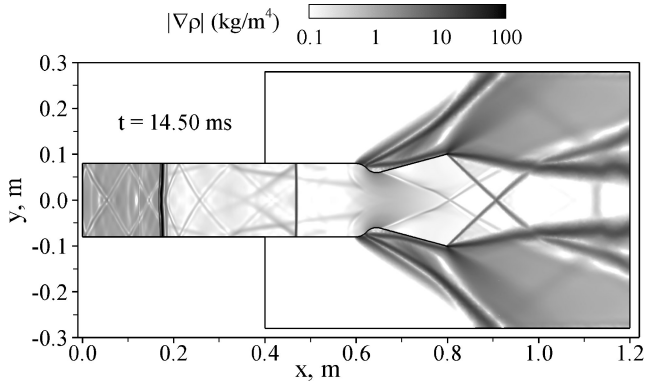

Fig. 12 Density-gradient field at $t = 14.5$ ms with ambient flow during steady periodic operation ($\tau_{cycle} = 3$ ms and $\tau_{close} = 2.1$ ms).

the nozzle is choked during most of the cycle period, thus helping preserve the chamber pressure.

In the preceding simulation case, the ambient flow is neglected, that is, the external flowfield is initially stationary and nonreflection boundary conditions are used. In reality, however, the strong ambient flow interacts with the nozzle exhaust gas and may affect the engine propulsive performance. To examine this effect, a supersonic inflow with a velocity of 636 m/s ($M_\infty = 2.1$) is applied at the left boundary of the external region (Fig. 2). Figure 12 shows the instantaneous density-gradient field at $t = 14.5$ ms and can be compared with the baseline case shown in Fig. 10e. In spite of the drastic change of the flow structure in the external region, the flowfield within the detonation tube and nozzle remains nearly identical. This can be attributed to the flow at the nozzle exit plane being supersonic during the whole cycle, and, as such, the ambient condition does not exert any influence on the chamber dynamics. Consequently, the specific thrust and impulse remain the same for cases with and without the ambient flow.

For comparison, simulations have also been conducted for an axisymmetric configuration with identical operating conditions and nozzle contours. The flow dynamics bear a strong resemblance to those of the baseline planar case, and the specific impulse is 3318 s.

B. Propulsive Performance

The propulsive performance of the PDE must be determined appropriately. Several experimental techniques have been employed to measure the impulse,[10] including the ballistic pendulum, load cell, damped thrust stand, spring–damper system, and integration of the pressure force on the thrust wall. In numerical simulations, the impulse or thrust can be obtained based on either the pressure force on the thrust wall or on the momentum balance for the entire system. The latter is more practical for engines including both inlets and nozzles, as detailed in the following paragraphs.

Given a control volume that encloses the engine as shown in Fig. 1, the momentum conservation gives

$$\int_{CV} \frac{\partial \rho \boldsymbol{u}}{\partial t}\,\mathrm{d}V + \oint_{CS} [\rho \boldsymbol{u}\boldsymbol{u}\cdot\boldsymbol{n} + p\boldsymbol{n}]\,\mathrm{d}S = 0 \tag{13}$$

where CV represents the control volume and CS the control surface, which can be further divided into three parts: the entrance plane S_i, the exit plane S_e, and the remaining surface S_w. By the definition of the mass flow rate $\dot{m}_e$, averaged velocity $\boldsymbol{u}_e$, and averaged pressure p_e at the exit plane as

$$\dot{m}_e = \int_{S_e} \rho \boldsymbol{u}\cdot\boldsymbol{n}\,\mathrm{d}S \tag{14}$$

$$\boldsymbol{u}_e = \frac{1}{\dot{m}_e}\int_{S_e} \rho \boldsymbol{u}\boldsymbol{u}\cdot\boldsymbol{n}\,\mathrm{d}S \tag{15}$$

$$p_e = \frac{1}{A_e}\int_{S_e} p\,\mathrm{d}S \tag{16}$$

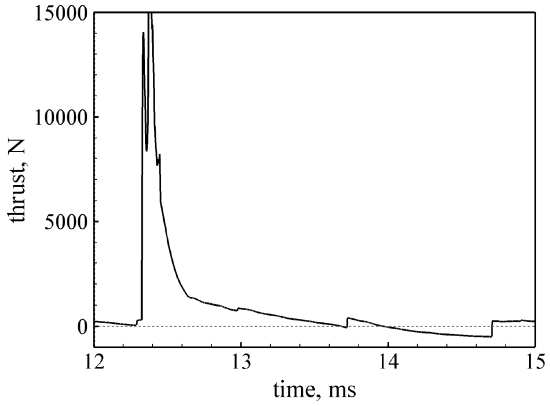

Fig. 13 Temporal variation of thrust during steady periodic operation (fifth cycle, $\tau_{cycle} = 3$ ms, and $\tau_{close} = 2.1$ ms).

the instantaneous thrust vector can be derived as

$$\boldsymbol{F} = -\{[\dot{m}_e\boldsymbol{u}_e - \dot{m}_a u_\infty \boldsymbol{i}] + [(p_e - p_\infty)A_e\boldsymbol{i}]\} - \int_{CV}\frac{\partial \rho \boldsymbol{u}}{\partial t}\,\mathrm{d}V \tag{17}$$

where $\dot{m}_a$ is the mass flow rate of air delivered to the inlet, or the cycle-averaged mass flow rate of air delivered to the combustor. For a steady periodic operation, the cycle average of the time-derivative term in Eq. (17) vanishes, and the cycle-averaged thrust becomes

$$\langle \boldsymbol{F}\rangle = -[\langle \dot{m}_e\boldsymbol{u}_e\rangle - \dot{m}_a u_\infty \boldsymbol{i}] - [(\langle p_e\rangle - p_\infty)A_e\boldsymbol{i}] \tag{18}$$

where the $\langle\,\rangle$ denotes the cycle-averaged quantity. Because of flow symmetry, the vertical component vanishes, and the axial component becomes

$$\langle F\rangle = [\langle \dot{m}_e u_e\rangle - \dot{m}_a u_\infty] + [(\langle p_e\rangle - p_\infty)A_e] \tag{19}$$

This formula is identical to that for steady engines, except for the use of cycle-averaged quantities. The two terms on the right-hand side are referred to as momentum and pressure thrust, respectively. The air-based specific thrust F_{sp} and fuel-based specific impulse I_{sp} are defined, respectively, as

$$F_{sp} = \langle F\rangle/\dot{m}_a, \qquad I_{sp} = \langle F\rangle/\langle \dot{m}_f\rangle g \tag{20}$$

Figure 13 shows the temporal variation of the axial thrust during a steady periodic cycle, which was obtained using only the first two terms in Eq. (17). The time variation of the chamber momentum was neglected. Thus, the result represents the effect of the exhaust flow, rather than the actual instantaneous thrust. The primary shock wave arrives at the nozzle exit at $t = 12.3$ ms, producing a jump in thrust. The negative thrust in the later part of the blowdown stage is caused by the low pressure and density at the exit plane. The thrust then becomes positive again when the shock resulting from the valve opening reaches the exit plane. The time duration of negative thrust is about 0.7 ms, from 14.0 to 14.7 ms. The cycle-averaged thrust is 862 N, and the specific thrust and specific impulse are 862 m/s and 3402 s, respectively. The system performance is much higher than that achieved with a straight tube, that is, $I_{sp} = 2328$ s (Ref. 2). The CD nozzle substantially improves the engine performance due to its effectiveness in preserving the chamber pressure during the blowdown and refilling stages, rather than the thrust produced by the nozzle wall itself. To verify this, the impulse generated by the nozzle section, obtained by integrating the pressure force on the wall and by applying momentum balance between the entrance and exit planes of the nozzle, is shown in Fig. 14. Both methods lead to the same result of a negative impulse of -0.716 N · s. The negative impulse has also been reported by Yungster[34] for divergent nozzles.

Note that the use of a single set of γ and R values throughout the entire thrust chamber, although calibrated against the CJ properties, may give rise to considerable discrepancies in predicting the flow properties during the blowdown process and, consequently, the

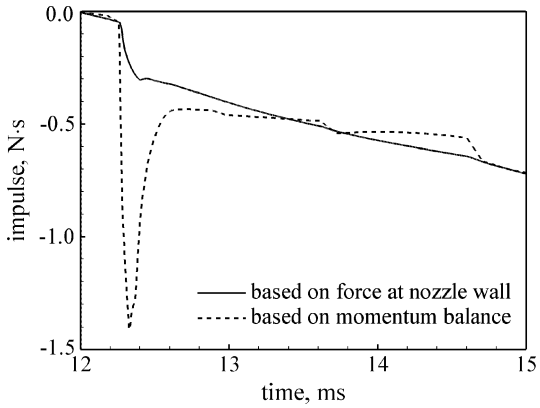

Fig. 14 Temporal variation of impulse produced by nozzle section during steady periodic operation (fifth cycle, $\tau_{cycle} = 3$ ms, and $\tau_{close} = 2.1$ ms).

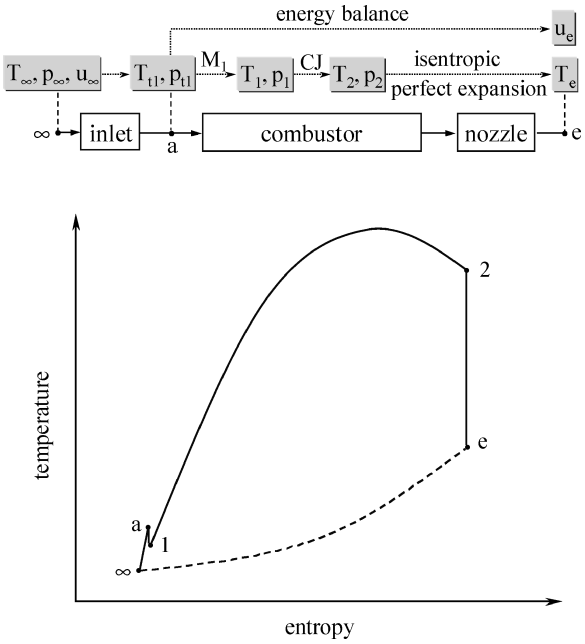

Fig. 15 Schematic of flowpath analysis and temperature–entropy diagram for PDE performance prediction.

propulsive performance. Harris et al.[35] recently demonstrated a large difference of engine performance predicted using one-γ and three-γ models. Extension of the single-γ performance analysis may be required to accommodate variable thermodynamic properties.

C. Analytical Prediction

It is desirable to develop a simple analytical model that can be used to assess the PDE performance effectively for comparison with numerical simulation results. Several analytical models summarized in Ref. 10 have been proposed and can be classified into two categories. The first uses unsteady gasdynamics theories to determine the impulse by time integration of the instantaneous forces acting on the thrust wall.[4,28] These models can only be applied to simple, straight detonation tubes with single-pulse operations. The second category obtains the engine impulse based on the flow properties at the exit plane.[2,36,37] The analytical model presented here closely follows the approach of Heiser and Pratt,[36] but takes into account the effects of the refilling velocity and the purging process to provide more accurate results. Figure 15 shows schematically the flowpath considered in the analysis and the corresponding temperature–entropy diagram. The subscripts ∞, 1, 2, and e represent the states of the freestream, unburned gas, CJ point, and exit plane, respectively. The procedure is outlined as follows:

1) Determine the total temperature T_{t1} and total pressure p_{t1} at the combustor entrance from the inlet flow analysis.

2) Obtain the static temperature T_1 and pressure p_1 of the refilled reactants by specifying a flow Mach number M_1.

3) Calculate the CJ temperature T_2 and pressure p_2 using Eqs. (7) and (8).

4) Calculate the exit temperature by assuming an isentropic flow expansion from the CJ state to the exit plane along with a perfect match with the ambient pressure:

$$T_e = T_2(p_\infty/p_2)^{(\gamma-1)/\gamma} \tag{21}$$

5) Deduce the exit velocity by applying the energy balance from the combustor entrance to the engine exit plane:

$$u_e = \sqrt{2[q - c_p(T_e - T_{t1})]} \tag{22}$$

6) Obtain the specific thrust and impulse:

$$F_{sp} = (1+f)u_e - u_\infty, \qquad I_{sp} = F_{sp}/(fg) \tag{23}$$

If the purging process is also included, the exit temperature can be determined based on the following equation:

$$T_e = (T_{e1}\cdot\tau_{purge} + T_{e2}\cdot\tau_{refill})/\tau_{open} \tag{24}$$

where τ_{open} is the valve-open period that equals the sum of τ_{purge} and τ_{refill}, and T_{e1} and T_{e2} are the temperatures obtained by assuming isentropic flow expansion from the purge-gas state (T_1, p_1) and the CJ state (T_2, p_2) to the exit plane, respectively:

$$T_{e1} = T_1(p_\infty/p_1)^{(\gamma-1)/\gamma}, \qquad T_{e2} = T_2(p_\infty/p_2)^{(\gamma-1)/\gamma} \tag{25}$$

The fuel-to-air mass ratio f in Eq. (23) should be replaced by its overall quantity $\bar{f}$:

$$\bar{f} = f\cdot\tau_{refill}/\tau_{open} = f(1-\beta) \tag{26}$$

where β is defined as the ratio of the purge to the valve-open time period:

$$\beta = \tau_{purge}/\tau_{open} \tag{27}$$

Similarly, the heat release q in Eq. (22) should include the effect of purge gas, taking the form

$$\bar{q} = q\cdot\tau_{refill}/\tau_{open} = q(1-\beta) \tag{28}$$

The specific thrust and impulse then become

$$F_{sp} = (1+\bar{f})u_e - u_\infty, \qquad I_{sp} = F_{sp}/(\bar{f}g) \tag{29}$$

Based on the preceding analysis, the specific thrust and impulse are functions of $\gamma, R, q, f, p_\infty, u_\infty, T_{t1}, p_{t1}, M_1$, and β. In the present study, the first eight parameters have fixed values of $\gamma = 1.29$, $R = 368.9$ J/kg·K, $q = 2.72\times10^6$ J/kg, $f = 0.0292$ (for stoichiometric H_2/air reactants), $p_\infty = 0.29$ atm, $u_\infty = 636$ m/s, $T_{t1} = 428$ K, and $p_{t1} = 2.12$ atm. The remaining two parameters, M_1 and β, can be optimized to achieve a maximum performance by selecting an appropriate engine operating sequence and system geometry. Table 2 lists the analytically predicted PDE performance for various

Table 2 Effects of refilling velocity and purge time on theoretical PDE performance

Condition, $p_{t1} = 2.12$ atm and $T_{t1} = 428$ K	F_{sp}, m/s[a]	I_{sp}, s[a]
1 $M_1 = 0$ and β[b] $= 0$	1246	4360
2 $M_1 = 0.93$ and $\beta = 0$	1167	4084
3 $M_1 = 0$ and $\beta = \frac{1}{9}$	1150	4527
4 $M_1 = 0.93$ and $\beta = \frac{1}{9}$	1075	4235
Baseline numerical results[c]	862	3402
Ramjet,[d] $\phi = 0.89$	903	3553

[a]Calculated from Eq. (29).
[b]$\beta = \tau_{purge}/\tau_{open}$.
[c]Calculated from Eq. (20).
[d]Calculated using the same gas as for the PDE.

refilling Mach numbers M_1 and purge-to-valve-open time ratios β. The result from the baseline numerical simulation, which has a time-averaged M_1 of 0.93 and β of $\frac{1}{9}$, is also listed for comparison. The first case, corresponding to an ideal situation with zero refilling velocity and no purging gas, has an I_{sp} of 4360 s. Both the specific thrust and impulse decrease with increasing M_1. This can be understood by using the aforementioned analytical formulas. As M_1 increases, T_1 decreases, leading to an increase in M_D, as given by Eq. (7). The combination of Eqs. (8), (21), and (22) indicates that T_e increases and u_e decreases as M_D increases, thereby reducing F_{sp} and I_{sp}. The decrease in performance with increasing M_1 can also be explained by the entropy generation across the detonation wave, which can be expressed as

$$\Delta s = s_2 - s_1 = c_p \ell_n \frac{T_2}{T_1} - R \ell_n \frac{p_2}{p_1}$$

$$= c_p \ell_n \left[\frac{1+\gamma M_D^2}{(1+\gamma)M_D^2} \left(\frac{1+\gamma M_D^2}{1+\gamma} \right)^{1/\gamma} \right]$$

$$\approx c_p \ell_n \left[\left(\frac{\gamma}{\gamma+1} \right)^{(\gamma+1)/\gamma} M_D^{2/\gamma} \right] \tag{30}$$

Furthermore, a larger M_1 leads to a stronger Taylor expansion and a lower head-end pressure and, consequently, a lower performance, a phenomenon recently observed by Wintenberger and Shepherd.[38]

The first and third cases in Table 2 indicate that F_{sp} decreases and I_{sp} increases with increasing β. The result is quite similar to the partial-filling effect[20,39] for single-pulse operation. A larger β translates to an increased air-to-fuel mass ratio. Part of the heat released from combustion is converted to the kinetic energy of the additional air, leading to a decrease in the exit velocity and, subsequently, the specific thrust. On the other hand, the overall fuel-to-air mass ratio $\bar{f}$, defined by Eq. (26), decreases faster than the specific thrust, causing an increase in specific impulse. The effect of β can be seen more clearly through the Taylor series expansion of F_{sp} and I_{sp} with respect to β:

$$F_{sp} = (1+\bar{f})u_e - u_\infty \approx F_{sp}^0(1 - A\beta) \tag{31}$$

$$I_{sp} = F_{sp}/(\bar{f}g) \approx I_{sp}^0[1 + (1-A)\beta] \tag{32}$$

where

$$A = \frac{1}{2} \cdot \frac{1 - c_p\left(T_e^0 - T_{e1}\right)/q}{1 - c_p\left(T_e^0 - T_{t1}\right)/q} \cdot \frac{u_e^0}{u_e^0 - u_\infty} \tag{33}$$

The superscript 0 denotes the quantity at the condition without any purge, that is, $\beta = 0$. For the current system, $A \approx 0.7$. Therefore, F_{sp} decreases and I_{sp} increases with increasing β. Furthermore, because $(1-A)\beta > A\beta$, the rate of increase in I_{sp} with respect to β is less than the rate of decrease in F_{sp}. From Table 2, when β increases from 0 to 1/9, F_{sp} decreases by 7.7% and I_{sp} increases by 3.8%. The result agrees well with the predictions from Eqs. (31) and (32).

The PDE performance is compared with its ramjet counterpart. In Ref. 2, the specific impulse of a ramjet with a stoichiometric hydrogen/air mixture was 3866 s. The product flow properties were obtained from the chemical equilibrium calculation[21] and had values of $\gamma = 1.177$ and $R = 341.4$ J/kg · K, which were different from those of the reactants ($\gamma = 1.4$ and $R = 396.6$ J/kg · K). If the same flow properties used in the PDE analysis, that is, $\gamma = 1.29$ and $R = 368.9$ J/kg · K, were employed for both reactants and products, and the product temperature was determined as

$$T_2 = T_1 + \bar{q}/c_p \tag{34}$$

then the ramjet I_{sp} became 3432 and 3553 s for the equivalence ratios of 1.0 and 0.89 (corresponding to the situation of $\beta = \frac{1}{9}$ for the PDE), respectively. The result apparently underpredicts the ramjet performance. Thus, flow properties must be carefully selected in a thermodynamically self-consistent manner to provide meaningful performance data.

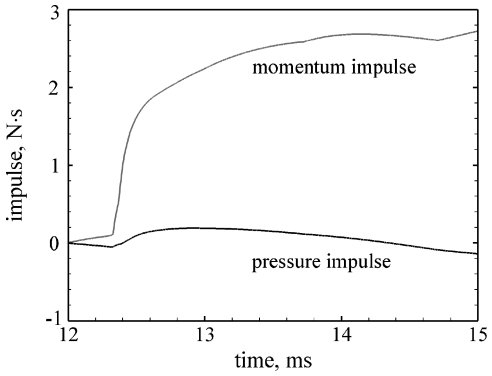

Fig. 16 Temporal variation of impulse during steady periodic operation (fifth cycle, $\tau_{cycle} = 3$ ms, and $\tau_{close} = 2.1$ ms).

D. Performance Loss Mechanisms

In addition to the performance degradation in the inlet and manifold, several loss mechanisms in the combustor and nozzle have been identified. These are attributed to viscous damping, wall heat transfer, refilling process, nozzle flow expansion and divergence, and chamber interior ballistics. The viscous damping and wall heat transfer losses are not considered in the current study. The performance loss associated with the refilling process has been discussed in the preceding subsection. As the refilling Mach number M_1 increases from 0 to 0.93, the specific impulse decreases by 6.5% from 4527 to 4235 s, as listed in Table 2. Note that, in reality, because of the nonisentropic expansion from the CJ state to the exit plane, the loss associated with nonzero refilling velocity cannot be isolated from other effects. It is, thus, estimated using the analytical model, Eq. (29). The other three loss mechanisms are responsible for the difference between the baseline numerical result and the analytical prediction, about 24.5% with respect to the numerical value of 3402 s.

For a conventional steady engine, the nozzle configuration is optimized in such a manner that the exit pressure matches the ambient state. This condition, however, cannot hold for PDEs due to their unsteady operation. The resultant performance loss, referred to as nozzle exit pressure mismatch loss, can be estimated by comparing the numerical calculation with the result of an idealized hypothetical situation in which the recorded exhaust flow is further compressed or expanded isentropically to allow for a perfect match with the ambient pressure. For the baseline case, this ideal specific impulse is 3604 s, and the nozzle expansion loss is about 6%. Figure 16 shows the temporal variations of momentum and pressure impulses during a steady periodic cycle for the baseline case. The pressure impulse, though much smaller than its momentum counterpart, is not zero as for an ideal situation. The nozzle is overexpanded from 12.0 to 12.3 ms and from 12.9 to 15.0 ms (indicated by the negative slope in the pressure impulse), and is underexpanded otherwise. At the end of the cycle, the momentum impulse and pressure impulse are 2.72 and -0.135 N · s, respectively, demonstrating a net effect of overexpansion of the nozzle flow.

The flow divergence loss results from the angularity of the exhaust velocity vector,[40,41] and is generally characterized by a nozzle divergence coefficient, defined as the ratio of the axial exhaust momentum to that from an ideal nozzle where the exhaust flow is uniformly parallel to the nozzle axis. For the current PDE system, the nozzle divergence coefficient can be expressed as

$$\eta_d = \left\langle \int_{S_e} \rho \boldsymbol{u} \cdot \boldsymbol{n} u \, \mathrm{d}S \right\rangle \Big/ \left\langle \int_{S_e} \rho \boldsymbol{u} \cdot \boldsymbol{n} \sqrt{u^2 + v^2} \, \mathrm{d}S \right\rangle \tag{35}$$

Equation (35) gives rise to a value of 0.987 for the baseline case, which is slightly lower than the analytical value for a steady two-dimensional nozzle flow with the same divergence half-angle of $\theta = 15$ deg:

$$\eta_d = \sin\theta/\theta = 0.989 \tag{36}$$

Table 3 Performance losses for baseline case[a]

Loss mechanism	Loss in I_{sp},[b] %	Loss in I_{sp},[c] %
Refilling process	8.5	6.5
Mismatch of nozzle exit pressure with ambient state	6.0	4.5
Nozzle flow divergence	2.0	1.5
Internal flow processes	16.5	12.5
Total	33	25

[a]Nozzle length = 20 cm, height = 12 cm, $\tau_{cycle} = 3$ ms, $\tau_{close} = 2.1$ ms, and $\tau_{purge} = 0.1$ ms.
[b]Relative loss based on baseline numerical result of 3402 s.
[c]Relative loss based on analytical prediction of 4527 s (condition 3 in Table 2).

In spite of the unsteadiness of the PDE exhaust flow, the flow divergence loss is about the same as that for conventional steady engines. Note that the nozzle divergence coefficient defined by Eqs. (35) and (36) does not include the effect of incoming airflow. If such an effect is taken into account, then the loss in net thrust becomes

$$\varepsilon_d = 1 - \left(\left\langle \int_{S_e} \rho \boldsymbol{u} \cdot \boldsymbol{n} u \, \mathrm{d}S \right\rangle - \dot{m}_a u_\infty\right) \Big/ \left(\left\langle \int_{S_e} \rho \boldsymbol{u} \cdot \boldsymbol{n} \sqrt{u^2 + v^2} \, \mathrm{d}S \right\rangle - \dot{m}_a u_\infty\right) \tag{37}$$

which leads to a value of 0.02 for the baseline case.

In the analytical performance prediction, the flow is assumed to undergo an isentropic expansion from the CJ state to the exit plane. In reality, complicated shock waves exist within the thrust chamber, as described in Sec. V.A. The resultant entropy increase and total pressure drop lead to a performance loss known as the internal flow loss, which can be estimated as 16.5% by subtracting the exit pressure mismatch and flow divergence losses from the overall loss. Table 3 lists the various losses for the baseline case. The large internal flow loss appears to be unique to PDEs.

E. Effect of Valve Timing

A parametric study was then conducted to investigate the effect of valve timing on the propulsive performance by varying the cycle time τ_{cycle}, valve-closed time τ_{close}, and purge time τ_{purge}. Figure 17 shows the effect of τ_{close} on the air-based specific thrust F_{sp} and the fuel-based specific impulse I_{sp} for three different cycle periods of 2.5, 3, and 4 ms, corresponding to operation frequencies of 400, 333, and 250 Hz, respectively. The purge time is fixed at 0.1 ms. Steady cyclic operation is achieved after 5–12 cycles in these cases. In some cases, when τ_{close} is small, the specific impulse reaches its steady value in a zigzag manner, in contrast to a monotonic increase for the baseline case.

For all of the frequencies considered herein, the specific thrust increases as τ_{close} decreases, a phenomenon that can be explained as follows. For a given τ_{cycle} and τ_{purge}, a smaller τ_{close} exerts the following five positive influences. First, the blowdown process becomes shorter and the resultant higher chamber pressure during the refilling stage elevates the loading density of fresh reactants. Second, the increased refilling period enhances the amount of reactants delivered to the chamber. Third, the duration of negative thrust is shorter. As pointed out in Sec. V.B, negative thrust may appear during the later part of the blowdown process due to the low-energy level of the gases in the combustor. Figure 18 shows the temporal variation of the thrust during a steady periodic cycle for different τ_{close}. When τ_{close} decreases from 2.4 to 1.8 ms, the time duration of negative thrust decreases from about 1.5 to 0.4 ms. Fourth, the refilling Mach number and the associated flow loss decrease. Finally, the internal flow loss becomes weaker. A smaller τ_{close} leads to a higher head-end pressure at the instant when the valve opens and, consequently, a weaker shock wave caused by the smaller pressure difference across the valve. In addition, the associated higher reactant temperature T_1 gives rise to a weaker detonation wave that subsequently reduces the internal flow loss arising from shock wave interactions in the chamber. The combination of the preceding effects render a rapid

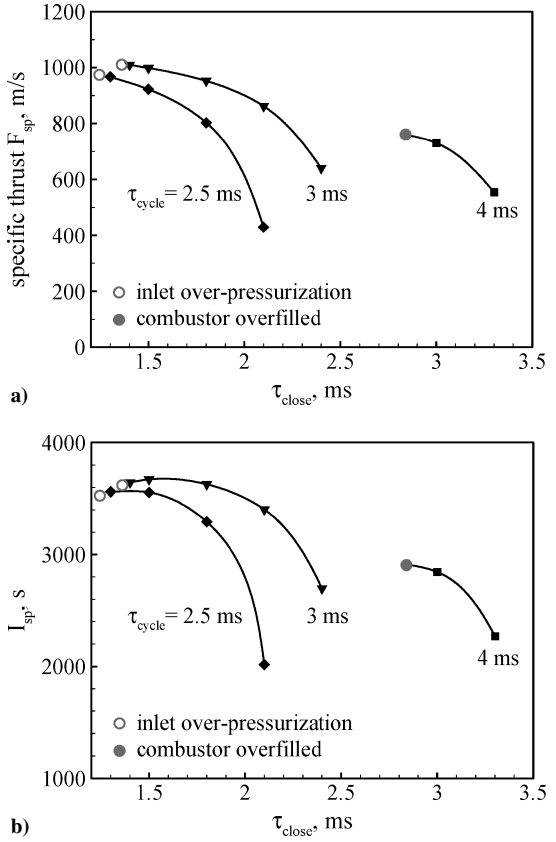

Fig. 17 Effects of valve-closed time on a) air-based specific thrust F_{sp} and b) fuel-based specific impulse I_{sp} for three different operation frequencies ($\tau_{purge} = 0.1$ ms, stoichiometric H_2/air mixture $h = 9.3$ km; and $M_\infty = 2.1$).

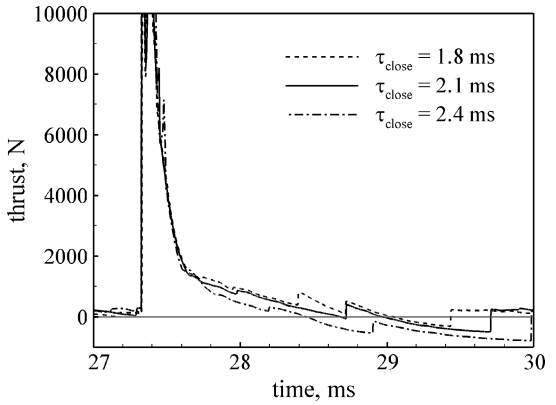

Fig. 18 Temporal variation of thrust during steady periodic operation (10th cycle, $\tau_{cycle} = 3$ ms, and $\tau_{purge} = 0.1$ ms).

increase in the specific thrust F_{sp} as the valve-closed time τ_{close} decreases.

Note, however, that a lower bound of τ_{close} often exists, subject to three practical constraints.[2] The first is concerned with inlet overpressurization, as denoted by the open circles on the curves with $\tau_{cycle} = 2.5$ and 3 ms in Fig. 17. The head-end pressure must not exceed the total pressure of the inlet air to allow for purging and refilling when the valve is open. Otherwise, reverse flow may occur and cause engine unstart. The second is related to chamber overfilling. The fresh reactants should be retained within the chamber before being burned completely unless afterburning is desired. This kind of lower bound usually occurs for low-frequency operations, as denoted by the filled circle on the curve with $\tau_{cycle} = 4$ ms. The third constraint, although commonly satisfied in practical cases, is that τ_{close} should be sufficiently long to cover at least the

time required for detonation initiation and propagation throughout the entire chamber. The upper bound of τ_{close} (also the lower bound of τ_{refill}) lies in the requirement that an appropriate amount of fresh reactants be delivered to the chamber to produce thrust.

The effect of τ_{close} on specific impulse follows the same trend as that of the specific thrust, except for a small range of τ_{close} near its lower bound. The specific impulse and specific thrust approximately satisfy the following relation:

$$I_{sp} = F_{sp}(1 + \tau_{purge}/\tau_{refill})/(fg) \tag{38}$$

As τ_{close} decreases, the factor $(1 + \tau_{purge}/\tau_{refill})$ decreases and may override the increase of F_{sp}, consequently leading to a decrease in I_{sp}, as shown in Fig. 17b.

Also observed in Fig. 17 is the existence of an optimum frequency. For a given τ_{close} and τ_{purge}, a lower operation frequency translates to a longer refilling period. As a consequence, a higher chamber pressure can be reached, and the engine performance improves. On the other hand, if the operation frequency is too low, τ_{close} must be increased accordingly to avoid chamber overfilling, and, thus, the performance is degraded. For the three frequencies considered herein, the 333 Hz ($\tau_{cycle} = 3$ ms) operation offers the best performance margin. The maximum specific impulse of 3672 s with $\tau_{close} = 1.5$ ms is 8% higher than that of the baseline case.

The effect of τ_{purge} on the propulsive performance was also studied. Figure 19 shows the specific thrust and impulse for different τ_{purge} with τ_{cycle} fixed at 3 ms and τ_{close} at 2.1 ms. Because τ_{open} remains constant at 0.9 ms, the effect of τ_{purge} is equivalent to that of β, as discussed in Sec. V.C based on analytical predictions. The present numerical results also indicate that the specific thrust decreases with increasing τ_{purge}, whereas the specific impulse increases with τ_{purge}. When τ_{purge} increases from 0 to 0.4 ms, the specific impulse increases by about 14%, but the specific thrust decreases by 37%. Both values are close to the analytical predictions of 13.3 and 31.1% from Eqs. (32) and (31), respectively.

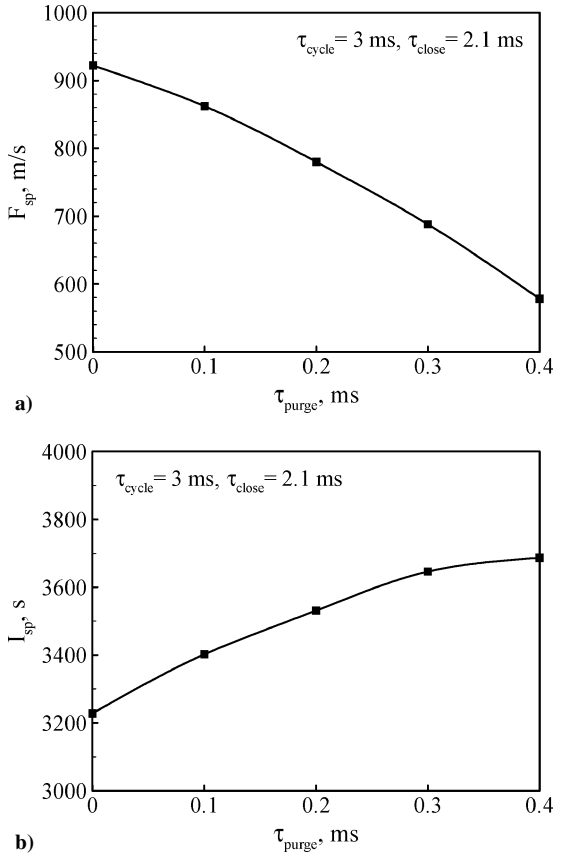

Fig. 19 Effect of purging time on a) air-based specific thrust F_{sp} and b) fuel-based specific impulse I_{sp} ($\tau_{cycle} = 3$ ms and $\tau_{close} = 2.1$ ms).

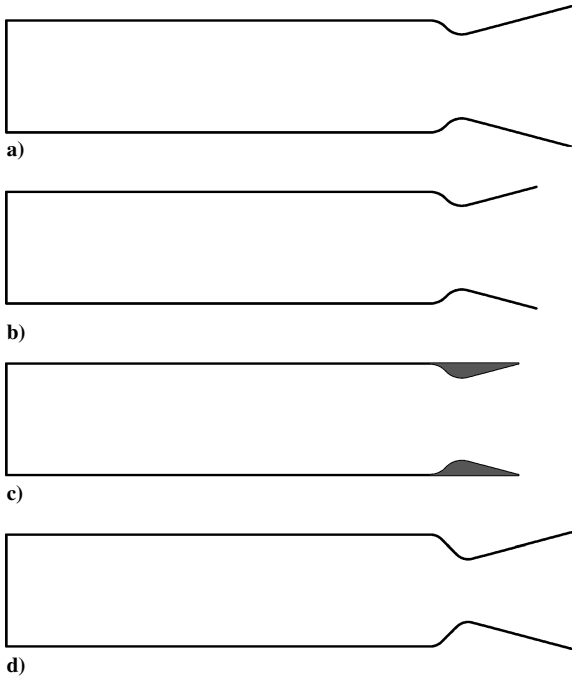

Fig. 20 Single-tube PDE configurations (tube length = 60 cm and tube height = 16 cm): a) baseline case, nozzle length = 20 cm, throat height = 12 cm; b) nozzle length = 15 cm; c) nozzle length = 12.4 cm; and d) throat height = 9 cm.

F. Effect of Nozzle Configuration

In addition to the operation timing, the nozzle configuration represents another important factor that affects the PDE propulsive performance. For conventional steady engines, the nozzle configuration is optimized by matching the exit pressure to the ambient condition. This simple criterion, however, is not easily applicable to PDEs because of their intrinsically unsteady operations. Several numerical[15,18] and experimental[19,20] studies have been reported on the effect of nozzle configuration on PDE performance. Most of them, however, are limited to single-pulse operation, and the issue of nozzle optimization is far from resolved. In general, a nozzle affects the engine performance through its influence not only on the gas expansion process, but also on the chamber dynamics. The coupling with the operation timing further compounds the problem.

Instead of conducting an extensive parametric study to optimize nozzle performance, which would require substantial computing resources, the present effort attempts to investigate the effects of nozzle configurations qualitatively. Emphasis is placed on CD nozzles. Figure 20 shows the four nozzle configurations with different lengths and throat areas considered herein. The baseline configuration, as described earlier, has a length of 20 cm and a throat height of 12 cm. In the second configuration, the nozzle length is reduced to 15 cm. The third nozzle has an even shorter length of 12.4 cm, with the exit area equal to that of the tube. The throat height of the fourth configuration is 9 cm, which is 25% smaller than that of the baseline nozzle. The expansion ratios of these nozzles are 1.68, 1.45, 1.33, and 1.85, respectively.

Simulations were conducted for all of the configurations with the same operation timing: τ_{cycle} of 3 ms, τ_{close} of 2.1 ms, and τ_{purge} of 0.1 ms. Figure 21 shows the temporal variations of the thrust and impulse during a steady periodic cycle. The corresponding performance parameters are listed in Table 4. The nozzle length plays a minor role in determining the PDE performance. The specific impulse decreases by about 1% when the nozzle length is reduced from 20 to 12.4 cm. The pressure impulse shown in Fig. 22 indicates that the overall effect of the second and third nozzles is underexpanded, that is, positive cycle pressure impulse, as opposed to overexpanded, that is, negative cycle pressure impulse, for the baseline case. For a nominal perfect-expansion nozzle, in the sense of zero cycle pressure impulse, the length should fall between 15 and 20 cm. Figure 23 shows the time history of the head-end pressure during a steady

Table 4 PDE performance with different nozzle configurations

Nozzle	F_{sp}, m/s	I_{sp}, s	Loss due to mismatch with ambient condition, %	Loss due to flow divergence, %
Baseline[a]	862	3402	6, Overexpansion	2.0
Length = 15 cm	860	3393	6, Underexpansion	2.5
Length = 12.4 cm	852	3365	7, Underexpansion	2.6
Throat height = 9 cm	917	3597	4, Overexpansion	2.0

[a]Nozzle length = 20 cm and throat height = 12 cm.

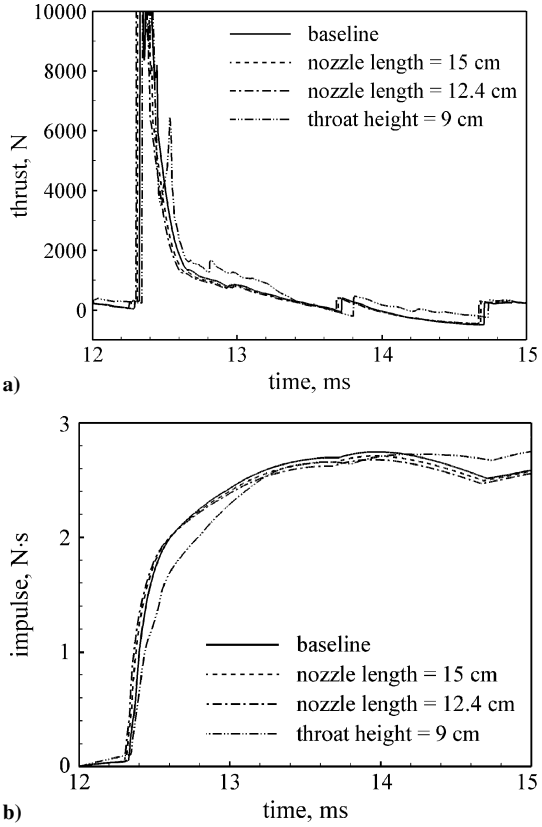

Fig. 21 Temporal variations of thrust and impulse during steady periodic operation (fifth cycle, $\tau_{cycle} = 3$ ms, and $\tau_{close} = 2.1$ ms).

periodic cycle. The curves for the first three cases coincide, suggesting that the nozzle length only affects the gas expansion process in the divergent section of the nozzle, not the gasdynamics within the detonation tube. The results also indicate a minor effect of the nozzle expansion ratio on performance within the range of 1.33–1.68 considered herein.

The nozzle throat area, on the other hand, exerts much more significant influences on the flow dynamics within the detonation tube as well as on the nozzle flow expansion process. The total impulse at the end of the cycle for a smaller nozzle throat, that is, the fourth configuration, is apparently higher than those for the other cases, as shown in Fig. 21b. The corresponding I_{sp} of 3597 s is 6% greater than that of the baseline configuration, a phenomenon that may be attributed to the following factors. A smaller throat helps preserve the chamber pressure, as evidenced in Fig. 23. The refilling pressure of 1.49 atm is higher than that of 1.24 atm for the other configurations. Consequently, the refilling Mach number is reduced from 0.93 to 0.76. The nozzle exit pressure mismatch loss is also reduced (Table 4). The relationship between propulsive performance and nozzle throat area is not monotonic. As the nozzle throat becomes exceedingly small, the internal flow loss arising from shock waves may increase substantially due to the severe geometrical constraints. Furthermore, a longer blowdown process may be required to avoid inlet overpressurization. A tradeoff between these two negative and the aforementioned positive effects will result in an optimum nozzle throat area for a given detonation tube configuration and operating parameters.

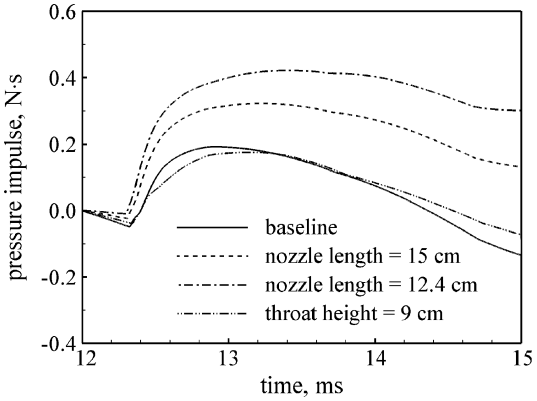

Fig. 22 Temporal variation of pressure impulse during steady periodic operation (fifth cycle, $\tau_{cycle} = 3$ ms, and $\tau_{close} = 2.1$ ms).

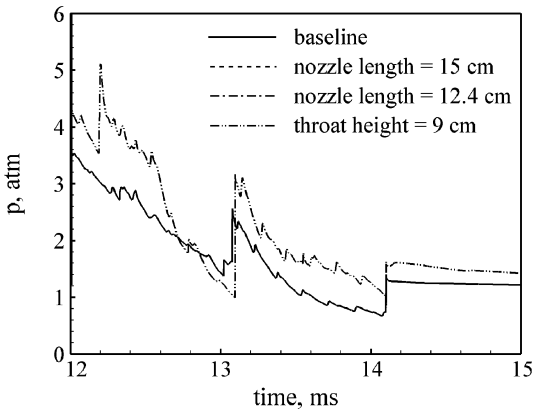

Fig. 23 Time history of head-end pressure during steady periodic operation (fifth cycle, $\tau_{cycle} = 3$ ms, and $\tau_{close} = 2.1$ ms).

Note that a performance analysis based on single-pulse operation may lead to totally different trends in terms of the nozzle effect. For example, during the first cycle, the net effect of all of the nozzle configurations considered herein is an underexpansion. The total impulse at the end of the first cycle for the baseline configuration is even higher than that for a smaller throat, which contradicts the conclusion based on steady periodic operation. Any realistic analysis of PDE performance must consider multicycle operations.

VI. Summary

The thrust chamber dynamics in a single-tube airbreathing PDE with repetitive operation has been studied both analytically and numerically. Various loss mechanisms limiting the engine performance, such as the refilling process, mismatch of nozzle exit pressure with the ambient condition, nozzle flow divergence, and internal flow dynamics, were identified and quantified. The effects of operating parameters and nozzle configurations were also investigated. In addition, a flowpath-based performance prediction model was developed to estimate the theoretical limit of the engine propulsive performance. The present work can be effectively utilized to optimize the PDE design and to provide practical means for further improvement.

A number of important conclusions drawn from this study are listed as follows:

1) The inherent mismatch of the flow conditions at the nozzle exit and the internal flow loss associated with the shock dynamics in the chamber are unique to PDEs as compared with conventional steady engines. These two loss mechanisms (about 6 and 16.5% for the baseline case, respectively) represent the primary factor degrading the PDE performance below its theoretical limit.

2) There exists an optimum operating frequency for achieving a best performance margin. For a given cycle period and purge time, the performance increases with decreasing valve-closed time in most cases. On the other hand, a larger purge time decreases the specific

thrust but increases the specific impulse for a given cycle period and valve-closed time.

3) The nozzle length plays a minor role in determining the engine performance because it only modifies the gas expansion process within the divergent section. The throat area, in contrast, affects the gasdynamics in both the nozzle and chamber, thus exerting a much more significant influence than the other geometrical parameters. Among the four nozzle configurations studied herein, the smaller throat improves the performance by up to 6%, whereas the nozzle length only affects the performance by 1%. A major factor contributing to the performance improvement with a smaller throat lies in the retaining of the chamber pressure during the blowdown and refilling processes. However, an exceedingly small throat may seriously jeopardize the engine performance due to the relatively longer blowdown process and larger internal flow loss.

4) Substantial differences exist between single-pulse and multicycle operations. Any realistic analysis of PDE performance must consider repetitive operations to provide more faithful results.

There are several important aspects that require extensive attention in the future. First, the employment of a single set of thermodynamic parameters, for example, γ and R, throughout the entire PDE thrust chamber inevitably introduces model errors that may considerably affect the performance prediction. Effort should be applied to accommodate variable thermodynamic parameters for reactants, products, and purge gases. Second, the unsteady operation of the manifold should be considered to provide more accurate flow conditions at the combustor entrance. Third, the characteristics of the valves for purge air and reactants should be treated separately. Fourth, the viscous damping and heat transfer losses in the chamber should be taken into account in the performance analysis.

Acknowledgments

This work was supported by the U.S. Department of Defense Multidisciplinary University Research Initiative under the U.S. Office of Naval Research Grant N00014-02-1-0589, with Gabriel Roy serving as the Program Manager. The authors are deeply grateful to Paul Harris for extensive discussions on the PDE performance.

References

[1]Kailasanath, K., "Recent Developments in the Research on Pulse Detonation Engines," *AIAA Journal*, Vol. 41, No. 2, 2003, pp. 145–159.

[2]Wu, Y. H., Ma, F. H., and Yang, V., "System Performance and Thermodynamic Cycle Analysis of Airbreathing Pulse Detonation Engines," *Journal of Propulsion and Power*, Vol. 19, No. 4, 2003, pp. 556–567.

[3]Hoffman, N., "Reaction Propulsion by Intermittent Detonative Combustion," Ministry of Supply, Volkenrode Translation, 1940.

[4]Nicholls, J. A., Wilkinson, H. R., and Morrison, R. B., "Intermittent Detonation as a Thrust-Producing Mechanism," *Jet Propulsion*, Vol. 27, No. 5, 1957, pp. 534–541.

[5]Dunlap, R., Brehm, R. L., and Nicholls, J. A., "A Preliminary Study of the Application of Steady State Detonative Combustion of a Reaction Engine," *Jet Propulsion*, Vol. 28, No. 7, 1958, pp. 451–456.

[6]Krzycki, L. J., "Performance Characteristics of an Intermittent-Detonation Device," U.S. Naval Ordnance Test Station, NAVWEPS Rept. 7655, China Lake, CA, 1962.

[7]Helman, D., Shreeve, R. P., and Eidelman, S., "Detonation Pulse Engine," AIAA Paper 1986-1683, June 1986.

[8]Eidelman, S., Grossman, W., and Lottati, I., "Review of Propulsion Applications and Numerical Simulations of the Pulse Detonation Engine Concept," *Journal of Propulsion and Power*, Vol. 7, No. 6, 1991, pp. 857–865.

[9]Kailasanath, K., "Review of Propulsion Applications of Detonation Waves," *AIAA Journal*, Vol. 38, No. 9, 2000, pp. 1698–1708.

[10]Ma, F. H., "Thrust Chamber Dynamics and Propulsive Performance of Airbreathing Pulse Detonation Engines," Ph.D. Dissertation, Dept. of Mechanical Engineering, Pennsylvania State Univ., University Park, PA, Dec. 2003.

[11]Kawai, S., and Fujiwara, T., "Numerical Analysis of First and Second Cycles of Oxyhydrogen Pulse Detonation Engine," *AIAA Journal*, Vol. 41, No. 10, 2003, pp. 2013–2019.

[12]Yungster, S., and Perkins, H. D., "Multiple-Cycle Simulation of a Pulse Detonation Engine Ejector," AIAA Paper 2002-3630, July 2002.

[13]Ma, F. H., Choi, J. Y., and Yang, V., "Thrust Chamber Dynamics and Propulsive Performance of Multitube Pulse Detonation Engines," *Journal of Propulsion and Power* (to be published).

[14]Oh, J. Y., Ma, F. H., Hsieh, S. Y., and Yang, V., "Interactions Between Shock and Acoustic Waves in a Supersonic Inlet Diffuser," *Journal of Propulsion and Power* (to be published).

[15]Cambier, J. L., and Tegner, J. K., "Strategies for Pulsed Detonation Engine Performance Optimization," *Journal of Propulsion and Power*, Vol. 14, No. 4, 1998, pp. 489–498.

[16]Cooper, M., Jackson, S., Austin, J., Wintenberger, E., and Shepherd, J. E., "Direct Experimental Impulse Measurements for Detonation and Deflagrations," *Journal of Propulsion and Power*, Vol. 18, No. 5, 2002, pp. 1033–1041.

[17]Sinibaldi, J. O., Brophy, C. M., Li, C., and Kailasanath, K., "Initiator Detonation Diffraction Studies in Pulsed Detonation Engines," AIAA Paper 2001-3466, July 2001.

[18]Eidelman, S., and Yang, X., "Analysis of the Pulse Detonation Engine Efficiency," AIAA Paper 1998-3877, July 1998.

[19]Daniau, D., Zitoun, R., Couquet, C., and Desbordes, D., "Effects of Nozzles of Different Length and Shape on the Propulsion Performance of Pulsed Detonation Engines," *High Speed Deflagration and Detonation, Fundamentals and Control*, edited by G. Roy, S. Frolov, D. Netzer, and A. Borisov, ELEX-KM Publishers, Moscow, 2001, pp. 251–262.

[20]Cooper, M., and Shepherd, J. E., "The Effect of Nozzles and Extensions on Detonation Tube Performance," AIAA Paper 2002-3628, July 2002.

[21]McBride, B. J., and Gordon, S., "Computer Program for Calculation of Complex Chemical Equilibrium Compositions and Applications," NASA Reference Publ. 1311, June 1996.

[22]Mohanraj, R., and Merkle, C. L., "A Numerical Study of Pulse Detonation Engine Performance," AIAA Paper 2000-0315, Jan. 2000.

[23]Wang, X. Y., and Chang, S. C., "A 2D Non-Splitting Unstructured Triangular Mesh Euler Solver Based on the Space–Time Conservation Element and Solution Element Method," *Computational Fluid Dynamics Journal*, Vol. 8, No. 2, 1999, pp. 309–325.

[24]Wu, Y. H., Ma, F. H., and Yang, V., "Space-Time Method for Detonation Problems with Finite-Rate Chemical Kinetics," *International Journal of Computational Fluid Dynamics*, Vol. 18, No.3, 2004, pp. 277–287.

[25]Karypis, G., and Kumar, V., "Multilevel K-Way Partitioning Scheme for Irregular Graphs," *Journal of Parallel and Distributed Computing*, Vol. 48, No. 1, 1998, pp. 96–129.

[26]Taylor, G. I., "The Dynamics of the Combustion Products Behind Plane and Spherical Detonation Fronts in Explosives," *Proceedings of the Royal Society of London, Series A: Mathematical and Physical Sciences*, Vol. A200, 1950, pp. 235–247.

[27]Fickett, W., and Davis, W. C., *Detonation Theory and Experiment*, reprint, Dover, New York, 2000, pp. 13–54.

[28]Wintenberger, E., Austin, J. M., Cooper, M., Jackson, S., and Shepherd, J. E., "An Analytical Model for the Impulse of a Single-Cycle Pulse Detonation Engine," *Journal of Propulsion and Power*, Vol. 19, No. 1, 2003, pp. 22–38.

[29]Han, Z. Y., and Yin, X. Z., *Shock Dynamics*, Kluwer Academic/Science Press, 1993, pp. 50–63.

[30]Hodge, B. K., and Koenig, K., *Compressible Fluid Dynamics with Personal Computer Applications*, Prentice–Hall, Englewood Cliffs, NJ, 1995, pp. 98, 99, 187, and 467–486.

[31]Skews, B. W., "The Shape of a Diffracting Shock Wave," *Journal of Fluid Mechanics*, Vol. 29, No. 2, 1967, pp. 297–305.

[32]Sun, M., and Takayama, K., "Vorticity Production in Shock Diffraction," *Journal of Fluid Mechanics*, Vol. 478, 2003, pp. 237–256.

[33]Skews, B. W., "The Perturbed Region Behind a Diffracting Shock Wave," *Journal of Fluid Mechanics*, Vol. 29, No. 4, 1967, pp. 705–719.

[34]Yungster, S., "Analysis of Nozzle Effects on Pulse Detonation Engine Performance," AIAA Paper 2003-1316, Jan. 2003.

[35]Harris, P. G., Ripley, R. C., and Guzik, S. M., "Single-Tube Two-Dimensional Evaluation of a Pulse Detonation Engine as a Ramjet Replacement," AIAA Paper 2004-3744, July 2004.

[36]Heiser, W. H., and Pratt, D. T., "Thermodynamic Cycle Analysis of Pulse Detonation Engines," *Journal of Propulsion and Power*, Vol. 18, No. 1, 2002, pp. 68–76.

[37]Talley, D. G., and Coy, E. B., "Constant Volume Limit of Pulsed Propulsion for a Constant γ Ideal Gas," *Journal of Propulsion and Power*, Vol. 18, No. 2, 2002, pp. 400–406.

[38]Wintenberger, E., and Shepherd, J. E., "A Model for the Performance of an Airbreathing Pulse Detonation Engine," AIAA Paper 2003-4511, July 2003; also *Journal of Propulsion and Power* (to be published).

[39]Li, C., and Kailasanath, K., "Partial Fuel Filling in Pulse Detonation Engines," *Journal of Propulsion and Power*, Vol. 19, No. 5, 2003, pp. 908–916.

[40]Berton, J. J., "Divergence Thrust Loss Calculations for Convergent–Divergent Nozzles: Extensions to the Classical Case," NASA TM-105176, 1991.

[41]Mattingly, J. D., *Elements of Gas Turbine Propulsion*, McGraw–Hill, 1996, pp. 804–809.